Current Status and Performance Analysis of Optical Camera Communication Technologies for 5G Networks

TRANG NGUYEN, AMIRUL ISLAM, MD. TANVIR HOSSAN, AND YEONG MIN JANG, (Member, IEEE)
Kookmin University, Seoul 02707, South Korea

Corresponding author: Y. M. Jang (yjang@kookmin.ac.kr)

ABSTRACT This paper investigates optical camera communication (OCC) technologies, targeting new spectrum, multiple-input-multiple-output diversity, transmission access, and novel architectures with augmented reality user experience for the extended 5G wireless network. It provides the current OCC research status and trend pertaining to these technologies, especially an inside view on the revision of IEEE 802.15.7-2011 known as the IEEE 802.15.7m (TG7m) Optical Wireless Communication Task Group. Such standardization activities have a major impact on the development of OCC technologies. In addition, it provides a detailed review of the related literature. Herein, OCC technologies are classified into five categories to elucidate their operations and technical characteristics. Furthermore, a concise performance analysis, numerical simulations, and some comparison of the results obtained for associated systems are presented, and the future directions of research and development are discussed.

INDEX TERMS 5G network, optical spectrum, optical camera communication, OCC, IEEE 802.15.7m, TG7m, modulation, coding, performance analysis.

I. INTRODUCTION

Fifth generation (5G) wireless systems represent the next generation of wireless communication systems. Although it is not yet entirely clear what next-generation technologies will offer, they could be related to higher data rates, improved spectral efficiency in systems, centralized controlling and provisioning, improved network capacity, greater scalability, more reliable modes of communication, and lower battery consumption and cost. Furthermore, 5G networks are expected to enable a wide range of new services that have high-end requirements, such as ultra-high-definition (UHD) video streaming, augmented and virtual reality, cloud gaming, smart homes, connected cars, and remote control of machines. Thus, 5G networks will need to support unprecedented demands in terms of data rates, latency, reliability, and energy efficiency for wireless communication to end-user devices while maintaining low-latency targets in order to ensure the delivery of real-time services. Developing solutions that can address these issues has become an extremely challenging task for network engineers. Although there are still debates about the direction of 5G technology, it is expected to be significantly different from existing communications technologies.

Optical wireless-based networking is expected to play a major supporting role in meeting the requirements for 5G technology and is expected to extensively change the existing infrastructure by reducing the deployment costs with the introduction of new technologies, such as new Physical layer (PHY) architectures, data links, network layer functionalities, and interfaces with different service layers. The aim of optical communication is to provide greater flexibility or adaptability to wireless networks by reducing the number of access points needed (*e.g.*, remote radio-frequency-based antennae). The important consideration when designing a network is how the capabilities and functionalities of the networks can be monitored and controlled. The introduction of software-defined networks (SDN) to 5G technology allows for centralized monitoring and control of an entire network [1]–[4]. Furthermore, advanced virtualization capabilities with network function virtualizations (NFVs) can
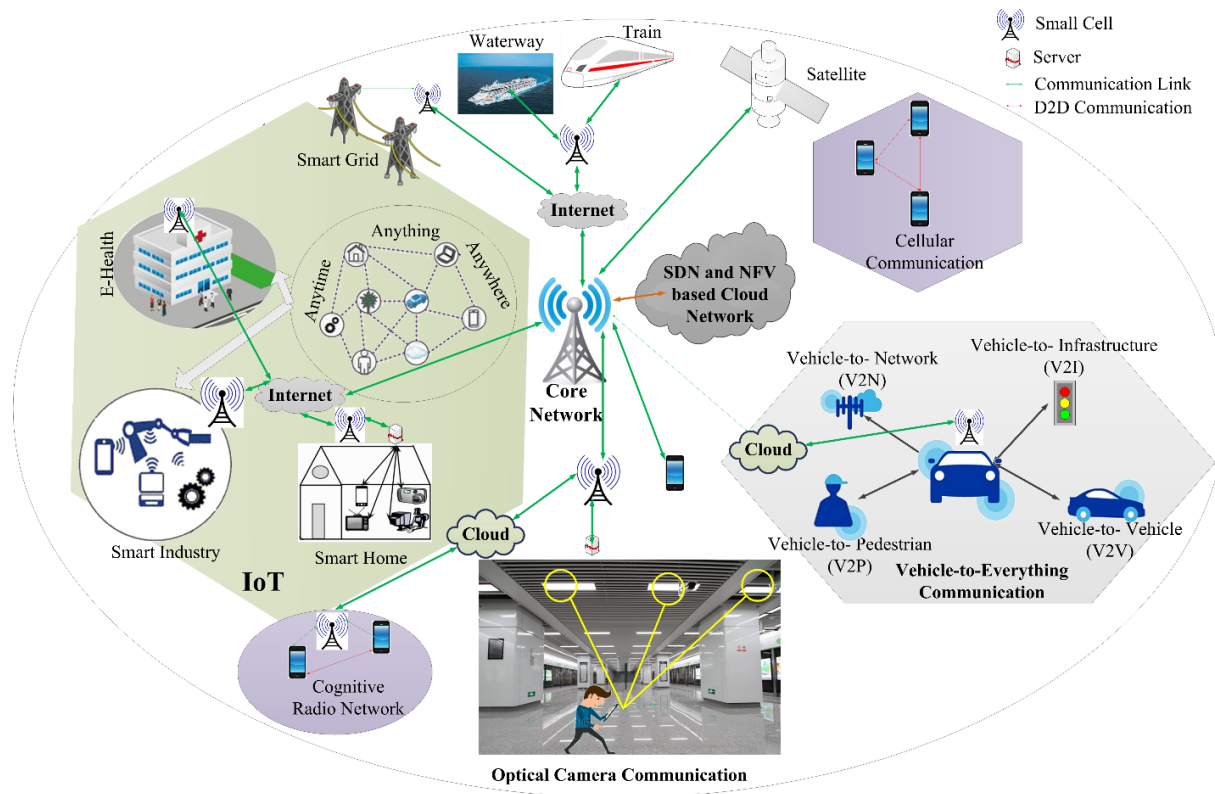
FIGURE 1. A multi-layer architecture for 5G networks with OCC and IoT.

prove advantageous for more centralized network architectures. The combination of SDN and NFV [5], [6] is expected to provide a lot of benefits such as cost reduction, reduced power consumption due to the consolidation of equipment, centralized provision of networks *via* the decoupling of the data plane from the network control plane, physical vs. virtual networking management, savings in terms of hardware, and cloud abstraction.

Conventional radio-frequency (RF)-based wireless communication systems have reached or are close to achieving their peak efficiency. They currently suffer from a shortage of spectra bandwidths because most frequencies have already been allocated. RF frequency utilization has been studied extensively, and the potential for further exploration is believed to be limited. Although low-power integrated-circuit (IC) innovations have helped improve power consumption, this is still a significant issue in RF communication. As such, researchers have been investigating alternative wireless commutation technologies. Visible-light communication (VLC), also known as optical wireless communication (OWC), is considered to be one such option, and it has attracted increasingly greater attention from academia and industry.

A. OVERALL 5G NETWORK ARCHITECTURE
This subsection presents the overall architecture of 5G network, figuring out the possibility of the usage of OWC technologies being coexistent with the current and

upcoming RF. Fig. 1 illustrates multi-layer architectures of 5G networks containing both existing and upcoming technologies, such as device-to-device (D2D) based communication, Internet of Things (IoT) clouds, cellular communication, optical camera communication, cloud-based communication, and vehicle-to-everything communication. As shown in Fig. 1, a core network monitors the entire network and small-cell or cloud-based networks work under the supervision of this core network; in essence, the core network acts as the backbone of the entire structure. Vehicular communication includes vehicle-to-vehicle, vehicle-to-infrastructure, vehicle-to-pedestrian, and vehicle-to-network communications, and these actors are all interconnected via a small-cell network. This system is connected to the core network through a cloud network.

Since the IoT is starting to play an important role in everyday life, it is expected to become a major part of next-generation 5G architectures. The architecture of the IoT incorporates smart industries, smart homes, e-health, and smart grids connected through the Internet; essentially, it is anything that can be made available anytime and anywhere. In future, it will be possible to monitor the movements of trains and ships through a core network. Cellular and radio communications will also be included in these centralized networks.

Finally, core networks that can be controlled by SDN- and NFV-based cloud networks will be able to provide centralized

TABLE 1. 802.15 projects with 5G potential

IEEE 802.15 Task Group	Operating bandwidth	Data rate	Distance	Benefit to 5G
802.15.3d 100Gbps	From 252 GHz to 325 GHz	100 Gbps	Few centimeter to several 100m	High data rate; traffic density up to several Tbps/km2; Cloud-RAN concepts.
802.15.7r1 Optical Wireless Communication, including: OCC, LiFi, and LED-ID	Wavelengths from 10,000 nm to 190 nm.	tens bps- tens Gbps	Several meter to hundreds meter	Spectrum is globally harmonized & unlicensed
802.15.8 Peer Aware Communication TG8	2.4GHz / 60GHz	10 Kbps to 55 Mbps	30m	Dynamically scalable data rate; cost effective.
802.15.4 LR-WPANs	Regional Sub-GHz bands	Tens kbps – 500kbps	Variable	Broadly used in IoT

services at both the user and application end because SDN provides scalable and secure centralized control of all systems through its interface [5], [6].

B. PROMISING TECHNOLOGIES FOR 5G

This subsection points out several promising technologies that can be used for 5G networking. Herein, the technologies for 5G networking have been discussed with standardization efforts.

1) IEEE 802.15 PROJECTS RELATED TO 5G

The IEEE projects related to 5G can be classified as shown in Table 1; the information was provided by Heile of the Wi-SUN Alliance. Four ongoing task groups of the IEEE 802.15 are attractive for 5G, including 802.15.3d Task Group, 802.15.7r1 OWC Task Group, 802.15.8 Peer Aware Communication Task Group, and 802.15.4 Low-rate Wireless Personal Area Networks (LR-WPANs) Task Group. Different characteristics (including the operating bandwidth, data rate, and distance) and multiple benefits to the 5G network have been addressed.

There are several solutions that could allow for an increased available spectrum and increased confinement of RF signals; WiGig is one such solution, as defined by IEEE 802.11ad, 802.11mc, 802.11aj, and the revised version of 802.11ay. However, the continued deployment and growth of 802.11 technologies relies on the utilization of unlicensed spectrums in order to satisfy complementary-use cases.

In this article, we only are focusing the promising technologies using optical wireless communication.

2) VISIBLE LIGHT COMMUNICATION FOR 5G

Currently, the majority of visible-light spectrums remain unused. They range from approximately 430–770 THz, which makes more than 1000 times the bandwidth of the entire RF spectrum (approximately 300 GHz) available for use. Since the visible-light and infrared (IR) spectrums are unlicensed, there is no cost for buying them.

While the current RF networks serve outdoor users or users in fast moving vehicles, VLC mainly serve indoor environment communications in future 5G systems because of the following factors (e.g., no interference between the different users due to different spectra, support communication and lighting at simultaneously). Therefore, VLC is an ideal implementation for micro-cell and attocell (approximately 1–10 m^2) as parts of the future 5G network [7]. VLC has experienced a lot of developments in the last few years. Extensive works have been performed on VLC [8], [9] and 5G [10], [11] individually but no significant connection has not been made between them. In the latter part of this section, the 5G network architecture with their promising technologies will be discussed.

Similar to VLC that utilizes visible light with unique features, LiFi (Light Fidelity) has the properties of small light interference, no signal from outside, easy to form beam with optics and due to line-of-sight facility it supports improved security [12]. Furthermore, LiFi spectrum is synchronized and unlicensed. The allocated Spectrum is non-interfering and promisingly complementary to the existing technologies in 802.11 and 802.15. Also, it creates no interferences and can be easily compatible with all the solutions of IEEE 802.11 and 802.15. As LiFi can ensure interference free, reliable communication, it attracts great attention both in academia and industries [12].

The main difference between VLC and LiFi can be described as follows. Undoubtedly, LiFi is more mature than VLC and has similar speed (up to 1Gb/s). VLC uses LEDs to transmit data wirelessly by using intensity modulation (IM). At the receiver, the signal is detected by a photodiode (PD) or camera. VLC has been conceived as a point-to-point data communication technique. Whereas LiFi includes bi-directional multiuser communication, i.e. point-to-multipoint and multipoint-to-point communication. LiFi also involves multiple access points forming a wireless network of very small optical attocells with the seamless handover. LiFi enables full user mobility, and therefore forms a new layer within the existing heterogeneous wireless networks.

VLC and LiFi both provide connectivity with low cost with using almost all the existing infrastructures. Both operate with no extra energy requirement in compared to the typical illumination devices, having comparable energy efficiency to RF technologies. Moreover, the feasibility of 100Gbps data rate over optical wireless communication has been discussed in [13]. Undeniably, the technology has satisfied the
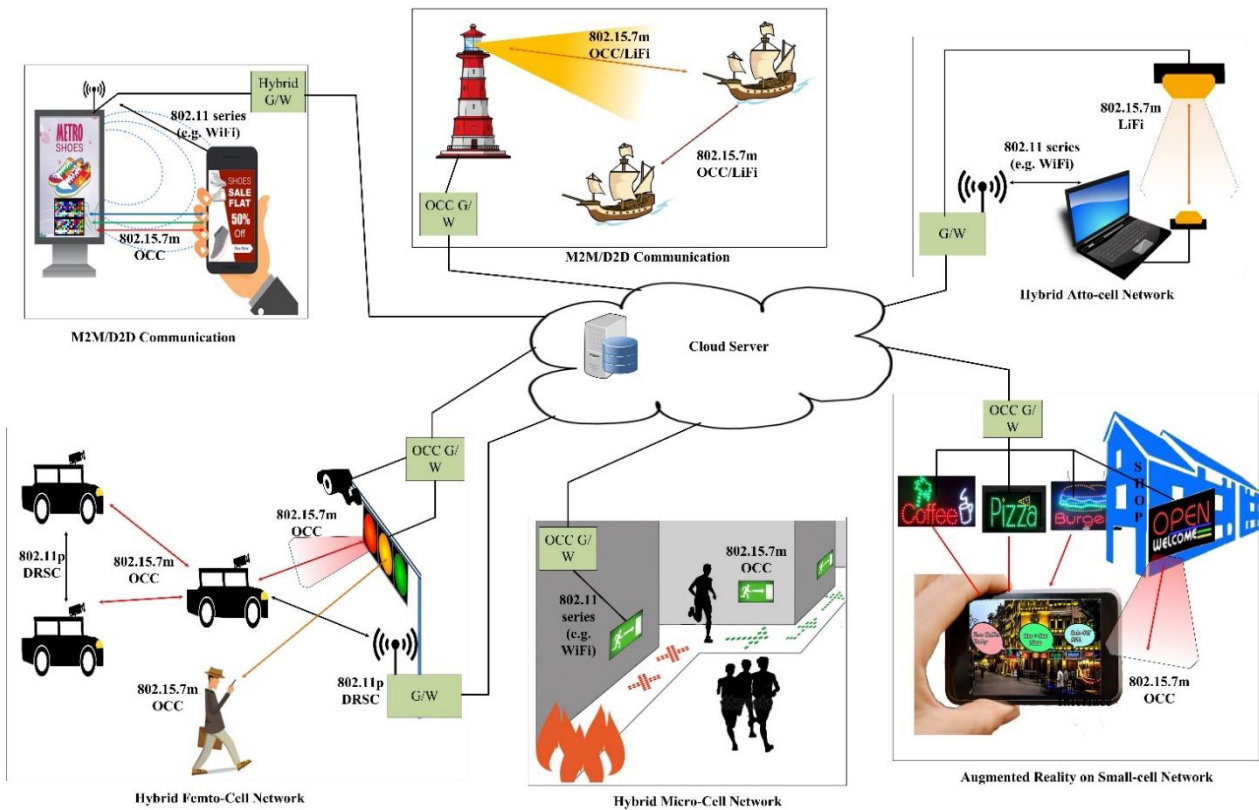
FIGURE 2. Example of IEEE 802.15.7m promising services for 5G.

requirement on new spectrum, data rate, device density, and delay, being coexistence and compatibility to the 5G network.

3) OCC TECHNOLOGY FOR 5G AND STANDARDIZATION

OCC is similar to VLC or LiFi in that it also relies on visible-light communication. The major difference between OCC and VLC is the receiver type; OCC uses a camera that comprises a two-dimensional array of photodiodes to receive demodulated light. Inheriting the achievement from VLC technology, OCC technologies that utilize an entire spectrum of light wavelengths (from IR to visible-light to ultraviolet (UV)) are widely applicable to applications such as augmented reality. The spatial separation characteristic of OCC is beneficial as well.

A range of OCC systems has been investigated. International standardization tends to exert a great impact on the development and research of a technology, and OCC is no different. TG7m OCC technologies are applicable to multiple applications and services, as illustrated in Fig. 2.

IEEE TG7m covers the infrared (700 nm–1 mm wavelengths), near-UV (100–400 nm wavelengths), and visible-light (400–700 nm wavelengths) spectra. It contributes the following technologies to revise the IEEE 802.15.7-2011 standard [14]:

- *OCC*: This allows for a scalable data rate, more specific positioning/localization, and message broadcasting

owing to the display and an image sensor being used as the transmitting and receiving devices, respectively.
- *LED-ID:* A wireless light identification (ID) system based on LEDs.
- LiFi: A high-speed, bi-directional, networked, and mobile wireless communication system that uses light.

Along with TG7m, the commercial feasibility of wireless communication using light has been addressed previously. Aside from its keen interest in LiFi and PureLiFi (UK), the

Fraunhofer Institute for Telecommunications (Germany) is involved in the development of both high-speed networks and small-cell mobile wireless communication networks. Intel (USA) has developed a killer app for OCC in the automotive industry. Panasonic (Japan) plans to open a service for OCC technology, known as online-to-offline marketing. Casio (Japan), Huawei Technologies (China), ETRI and LG Electronics (both Korea), and China Telecom (China) have all professed their interest in these technologies and are developing their own variants. Furthermore, several academic researchers from a number of different countries, including Ozyegin University (Turkey), Seoul National University of Science and Technology (Korea), California State University Sacramento (USA), Kookmin University (Korea), Istanbul Medipol University (Turkey), the National University of Taiwan (Taiwan), and Fudan University (China) have all presented technologies with high technical feasibilities.

TABLE 2. A classification of OCC modulation techniques.

Modulation schemes	Flicker modulation	Flicker-free modulation			
	Class A	Class B	Class C	Class D	Class E
	Nyquist sampling	Frame-rate Nyquist sampling	RoI Under-sampling	Hybrid OCC/PD	Rolling Shutter Sampling
1. PixNet by S.D. Perli *et al.* [15] 2. COBRA by T.Hao *et al.* [16] 3. Color Shift Keying and CDMA [17] 4. **TG7m** Picapi camera app [18] 5. Hierarchical scheme MIMO RGB-LED [19] 6. Microsoft LightSync color code [20] 7. **TG7m** 2D-sequential color codes [21] 8. **TG7m** Invisible data embedding codes [22] 9. HiLight by W. A. Cahyadi [23] 10. Image based Barcodes and watermarks [24] 11. Polarized light modulation [25] 12. Structure-light-assisted OWC [26]	✓				
13. A-On-A'-Off protocol [27] 14. Space Shift Keying [28] 15. 3/2 Oversampling scheme [29] 16. Layered Space-Time Code [30] 17. Hierarchical Rate adaption Scheme [31] 18. Erasure Coding [32]		✓			
19. **TG7m** UFSOOK twinkle VPPM [33–34] 20. UPSOOK by Luo *et al.* [35–37] 21. **TG7m** Spatial 2-PSK and HS-PSK [38–39]			✓		
22. Manchester coded OCI by Isamu Takai [40–41] 23. Optical-OFDM OCI by Yuki Goto et al [42–43]				✓	
24. **OOK** Manchester coding by PureLiFi [44] 25. OOK based Light Encryption Scheme [45] 26. **TG7m** Compatible OOK [46] 27. **TG7m** PWM/PPM code [47–48] 28. M-FSK by CMU [49] 29. **TG7m** Rolling Shutter-FSK [50–51] 30. **TG7m** Compatible M-FSK [52–53] 31. **TG7m** Hybrid M-FSK/2-PSK [52–53]					✓

Recently, in January 2017, the initial integration of technologies was formed, subject to comment and resolve.

The rest of the article is organized as follows. Section II presents the overview of promising OCC technologies whereas Section III describes the channel modeling of OCC technologies. Then Section IV presents the reference architectures, and performance evaluation of screen based Nyquist sampling and Section V describes the high frame-rate Nyquist sampling. Section VI represents the reference architecture and performance comparison of RoI (region-of-interest) signaling techniques. The Hybrid OCC and PD communication system have been presented in Section VII and the rolling shutter sampling reference architecture with their performance comparison has been discussed in Section VIII. Finally, Section IX concludes our article with the future direction.

II. OVERVIEW OF OCC TECHNOLOGIES

A range of modulation and coding schemes have been investigated for use in OCC systems because they are considered to be the key drivers in a communication system's performance. A suitable modulation scheme depends on the image sensor used, the method by which the exposure is made, and the light source used. However, constructing a classification of modulation schemes and systems solely based on the characteristics of the light source or image sensor would prevent an acceptable classification from being derived.

Table 2 summarizes the most cited pieces of research on OCC, classifying the schemes into five major categories based on the following technical considerations. (i) The characteristics of modulated light as perceived by the human eye. This consideration suggests the proper use of light sources along with any modulations and is necessary because the primary purpose of a light source is to illuminate, with communication being a secondary concern. (ii) The method by which the camera receiver (Rx) demodulates data (the type of camera used to acquire the data when the limitation imposed on the communications system is based on the camera receiver rather than the transmitter (Tx)).

A. NYQUIST SAMPLING BASED FLICKER MODULATIONS

The modulation of a screen transmitter is not restricted to any particular flicker frequency because the flickering of a screen is less troubling for the human eye compared with the flicker

from a LED; thus, the optical clock rate at which a block of a two-dimensional (2D) code is clocked out can be achieved even at low frequencies, such as 10 or 20 Hz.

Obviously, the optical clock rate must be less than the typical frame rate of a camera (i.e., 30 fps), and being satisfied the Nyquist sampling theorem. Several notable screen-based OCC methods and systems are listed in category A, which describes flicker modulation, as shown in Table 2.

PixNet and COBRA codes are remarkable for screen modulation. PixNet, developed by S. D. Perli *et al.* [15], encodes data in the frequency domain by adopting a 2D Orthogonal Frequency-Division Multiplexing (OFDM) modulation scheme. The throughput can be in the range of several Mbps, but the processing time is limited by the low optical clock rate, which has a transmission of no more than 5 Hz,*i.e.,* five blocks per second [16]. COBRA, developed by Hao *et al.* [16], uses a novel 2D barcode that has been optimized for the real-time streaming of data using five colors and three further optional colors at a clock rate of around 10 Hz. The issue of a lack of synchronization between the framerates of the transmitter and the receiver was resolved using Microsoft LightSync [20], which uses interframe coding to support asynchronous communication.

The time-variant frame rate problem is also taken account of in the TG7m technical proposals on screen modulation, which include the use of 2D-sequential color codes [21] and Casio Picapi camera [18]. TG7m screen modulations target the optimization of the transmission overhead over time sequential protocol, allowing a wide range of image sensors to be supported. Existing TG7m modulations are mostly designed to support tens of kbps data rate operating at 10 Hz optical clock rate, to accommodate cameras with lower frame rates of 20 fps. Future work will seek to update the TG7m screen modulation technologies to allow efficient and reliable communication. Moreover, a process for merging similar methods is also being discussed by the TG7m committee.

Changes in the intensity of light used in invisible data-embedding techniques are imperceptible to the human eye. However, there are a lot of similarities between 2D-sequential coding and invisible data-embedding techniques [22]–[24] that modulate a screen light source; for instance, both make use of optical clock rates that are lower than the eye cut-off frequency and employ similar data mapping techniques. Hence, both 2D-sequential and invisible data-embedding codes are placed in the flicker-modulation category.

Hereafter, there are still related works associated with screen modulations that modulate the screen in a different way. For example, a modulation inspired by the design of LCD screen, proposed by Jiansong Zhang *et al.* (Microsoft Research Asia) presented an approach called polarized light modulation, inspired by the design of the LCD screen [25]. A drawback of this approach is that an additional polarizer must be placed in front of the camera receiver to demodulate the polarized light. Furthermore, some image watermarks/data embedding approaches have been proposed, for

example in [23] and [24], which may be included in the updates of technical proposals using invisible codes.

B. HIGH-FRAME-RATE NYQUIST SAMPLING

Given that illumination is the primary purpose of a light source, in some applications, such as in vehicles, light must be flicker-mitigated. This requires the optical modulation rate to be greater than 200 Hz because this makes the changes in the intensity of the light imperceptible to human eyes [54]. For the camera samples operating at a frequency (equal to the frame rate) that is several times higher than the modulation rate, a several-hundred-fps or a kilo fps (kfps) frame rate camera should be used.

High-speed cameras address the demodulation of light modulated at hundreds of Hertz by using the Rx–Tx over-sampling ratio, as described in the schemes shown in Table 2. For example, in one scheme, a high-speed camera-based transmission protocol uses an A-On-A'-Off protocol [27] (where A' is the inverse of a block of data, A) that is similar, in principle, to differential coding. A space-time code called Spatially-Modulated Space-Time (SM-ST) proposed by Ebihara *et al.* [28] used two blocks of 2x2 LED matrices to transmit 3 bits. An updated protocol for a 2N×2N LED matrix, called Layered Space-Time Code, then allowed multiple LEDs to be used, and the data rate adapted to handle variations in distance [30]. All the above mentioned studies used high-speed cameras (1000 fps) for vehicular applications. Other notable techniques, such as hierarchical rate adaption schemes using wavelet transforms [31], allow for the incorporation of four-level priority in data mapping. The camera Rx can then adapt the amount of data demodulated based on the image resolution at different distances. Additionally, an erasure code that detects and recovers frames that are lost by the unsatisfied oversampling of framerates is notable [32]. Although these studies have demonstrated the reliable performance of high-framerate processing, the cost of the high-speed cameras required makes them an unattractive proposition.

C. REGION OF INTEREST SIGNALING

As oversampling requires the use of a high-speed camera Rx, a heavy computational burden is imposed in detecting the light source Tx(s) and demodulating the data. However, the high-frame-rate processing schemes are cost-ineffective. The RoI, a technique familiar to camera developers, may be applied to camera Rx, allowing a high frame rate to be achieved while minimizing the computational cost simultaneously. Thus, the methodology in implementing RoI based communication is one of the three PHY operating categories for OCC within IEEE TG7m (see Table 2).

The RoI signaling technique uses the simultaneous transmission of two data streams: (i) a low rate stream that is used to detect the RoI, and then (ii) high-rate stream is transferred via the selected RoI. This is performed by using a RoI-camera that utilizes the detected RoI to accelerate the frame rate and to demodulate the data at high speed. Demodulation of

two streams can be assigned to a pair of cameras or a single programmable camera. For a dual camera system, the first camera can detect the RoI and set up the link for the second demodulating the data at high speed simultaneously. Considering the cost-effectiveness of this approach, a low frame-rate (e.g. 30fps) camera is used to extract the RoI information.

1) ROI SIGNALING LOW-RATE STREAM

An innovative modulation scheme to blink the light source indication has been introduced by R. D. Roberts (from Intel) initially and contributed to TG7m [33], [34]. The modulation called Undersampled Frequency Shift On-Off Keying (UFSOOK), it is undersampled, flicker-free, and can be used by low-speed cameras at 30fps. UFSOOK is a form of DC balanced differential coding; it functions in a manner similar to FSK, and its undersampling characteristics allow for bits to be encoded at flicker-free frequencies while being simultaneously and successfully decoded by a low-framerate camera (*e.g.*, 30fps). Notably, it allows for the use of both global-shutter and rolling-shutter cameras. This compatibility with both shutter types and low-framerate cameras is the key to the usefulness of UFSOOK.

Another undersampling scheme known as Undersampled Phase Shift On-Off Keying (UPSOOK), was introduced by Luo *et al.* [35]–[37] and it also displays a remarkable level of performance. In the UPSOOK system, Rx demodulates a bit from two sampled images in the same manner as UFSOOK such that the camera frame rate is twice the bit rate.

Undersampling can also be performed spatially using a spatial modulation scheme called Spatial 2-Phase Shift Keying (S2-PSK), which has recently contributed to TG7m [38], [39]. The spatial separation capacity of the camera allows S2-PSK to fully demodulate a bit within a randomly sampled image. The support for the demodulation under random sampling allows for this approach to be used with time-variant frame rate cameras, which extends its compatibility to a wide range of image sensors.

2) HIGH RATE MIMO DATA STREAM

This sub-section explains hybrid modulation of the RoI data stream and high-rate Multiple-Input-Multiple-Output (MIMO) data stream.

Twinkle VPPM [34] is a combination of UFSOOK and VPPM. The amplitude modulation (AM) signal is generated in VPPM by changing the duty cycle of the groups of high rate pulses (via pulse width modulation) over time. This imparts a low-frequency UFSOOK amplitude envelope to the high rate data so that the LED light appears to change its intensity in a low-frequency manner while still transmitting at a high data rate. The low-frequency amplitude envelope makes the LED light appear to flicker (twinkle), and this is used as a beacon to identify LEDs that are transmitting high rate data.

Hybrid Spatial Phase-shift Keying (HS-PSK) [39] is a dedicated combination of S2-PSK and dimmable spatial multiple-PSK (DSM-PSK). Similar to the Twinkle VPPM, the AM signal that forms the basis of S2-PSK is generated using DSM-PSK. DSM-PSK comprises multiple VPPM signals with delays, it dims the light source by changing the duty cycle, and generating even intervals of low dimming and high dimming, creating a low-frequency AM signal at 200 Hz or 125 Hz. The AM signal is modulated using the S2-PSK encoding rule.

Also introduced by Intel to TG7m, Near-Infrared light (NIR), particularly at the 850 nm wavelength, and with a link budget up to 16 kbps [34], objects to use in automotive positioning/augmented reality applications.

D. HYBRID OCC AND PD COMMUNICATION

Several studies have investigated hybrid OCC and Photodiode (PD) systems [40]–[43] that are able to realize new types of image sensors with PD cells (*i.e.*, communication cells) integrated between the image pixels (*i.e.*, image cells). An image output from image cells is used to detect the light source, and a communication link is subsequently set up and the PD cells are activated.

The technique also requires the detection of RoI; however, RoI signaling is not investigated, and Computer Vision based RoI detection is performed instead. If the RoI is assumed to have been successfully detected, the PDs within the selected RoI are activated and are ready for the demodulation of the PD communications. By using a novel architecture for the image sensor, the frequency response of the PD cells in the image sensor can be tested [43] and several PD communication methods can be implemented, including baseband modulations with line coding [40], [41] and OFDM [42], [43].

Inheriting the achievement of PD communications from existing VLC standards such as IEEE 802.15.7-2011 std. [55], along with the achievement of high-rate PD communication sub-committee (LiFi sub-committee) in the ongoing IEEE 802.15.7 revision TG7m [56], [57], hybrid OCC and PD communication systems are considered to be a promising research direction as they benefit from the spatial separation of OCC and the "5G required data rate" of LiFi.

E. ROLLING SHUTTER BASED OCC

Being a part of non-flicker modulation series, with the vast usage of rolling shutter cameras in the camera market, the use of rolling shutter cameras in OCC systems takes advantage of the high sampling rate of the rolling shutter mechanism, which sequentially exposes lines of pixel to the incoming light. The Rx sampling rate of these systems, which reflects the pixel sampling rate of the rolling shutter, is much higher than the Tx optical clock rate. In principle, the frame rate of a high-speed camera Rx must be greater than the Tx optical clock rate to satisfy the Nyquist rate. An analysis of the relevance of the image sensor parameters (such as readout time, exposure time, and rolling shutter sampling rate) to communication applications has been presented [46].

Table 2 includes the modulation schemes for rolling shutter OCC systems submitted to TG7m and presented in related works. These include the following technical

TABLE 3. Performance estimation of OCC technologies and intended systems.

Performance	Class A Nyquist sampling	Class B Frame-rate Nyquist sampling	Class C RoI Under-sampling	Class D Hybrid OCC/PD	Class E Rolling Shutter Sampling
Distance	Several meter	hundred meter	hundreds meter	hundred meter	Several meter
Data rate	kbps-Mbps (visual MIMO)	Tens kbps	Tens kbps	Up to Gbps	< kbps
Intended Systems and Services	• Screen Tx • Typical cameras Rx	• Traffic light Tx • High-speed camera Rx	• Car light/traffic light Tx • RoI camera Rx	• Car light/traffic light Tx • New image sensor	• LED panel Tx • Rolling shutter camera Rx
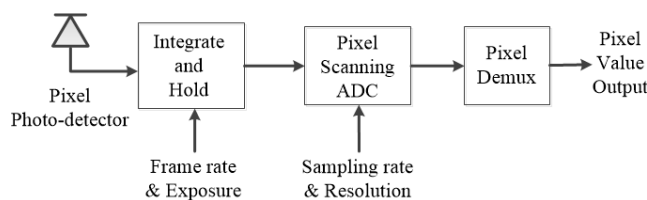
1- Frame rate & Exposure are setups for Integrate Hold functional block. This block affects to the limited bandwidth for communications.

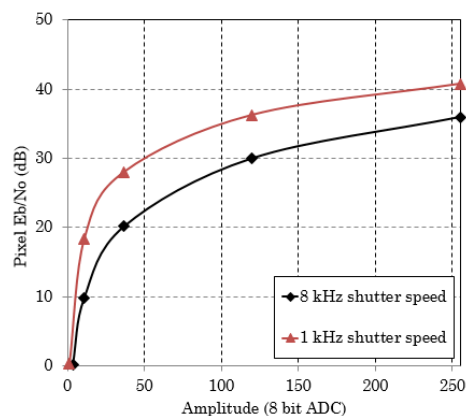2- Sampling rate & Resolution (or Region of Interest mode) are setup for Pixel Scanning ADC functional block.

(a)

(b)

FIGURE 3. Image sensor modeling. (a) Image sensor block diagram. (b) Relationship between pixel amplitude and E_b/N_0.

proposals that were submitted to TG7m: compatible OOK (C-OOK) from Kookmin University, Pulse Width/ Position Modulation (PWM/PPM) code from Panasonic, rolling shutter-FSK (RS-FSK) from National Taiwan University, and the compatible M-FSK series (CM-FSK) from Kookmin University. The related works discuss OOK based line coding developed by PureLiFi [44] and M-FSK developed by Carnegie Mellon University [49].

The highlighted works presented in Table 2 can be grouped into two types: time modulation series (OOK schemes [44]–[46] and PWM/PPM [47], [48]), and frequency modulation series (M-FSK schemes [49], [52], [53], and RS-FSK [50], [51]). The modulations listed by TG7m were designed to be compatible with a wide range of image sensors, whereas those presented in the related works did not take into account the compatibility considerations. In particular, C-OOK [46] enables the detection of packets that are missing because of a sharp decline in the Rx frame rate. A pair of asynchronous bits (Ab) allows for the detection of two-thirds of these missing packets. Two other modulation schemes, RS-FSK [51] and CM-FSK [52], are compatible with cameras that have widely different frame rates, readout-times, inter-frame gap times, and pixel sampling rates. The typical bandwidth of smartphone cameras is also supported. Moreover, PWM/PPM is designed to support bandwidths of ≥10 kHz, which facilitates greater data rates.

All of these rolling-shutter-based OCC systems share a problem that results from the trade-off between the data rate and the communication distance; this trade-off means that the amount of data available is proportional to the resolution of the light source on the image. A detailed analysis of the performance shall be discussed fully in the following sections. From our perspective, these modulation schemes are most suitable for indoor scenarios or for smartphone users located in nearby buildings because the distance is usually no more than 10 m and the camera receiver is equipped with a pedestrian's smartphone. Researchers have shown that the rolling shutter OCC technology is to deliver accurate indoor localization and navigation [58], [59], or some other promising services [60], [61] for inside buildings where GPS cannot reach.

A brief comparison of the performance and intended services of the five categories of OCC systems is given in Table 3. The discussion on how these performances are achieved is presented throughout this paper.

III. OCC CHANNEL MODELING
A. IMAGE SENSOR MODELLING
Before moving to the calculation of E_b/N_o, *i.e.*, to evaluate and compare the performance of the modulation and coding techniques, the model of the image sensor as a 2D light wave-to-digital converter is shown in Fig. 3(a). In this model, all possible parameters which control image sensors/cameras are
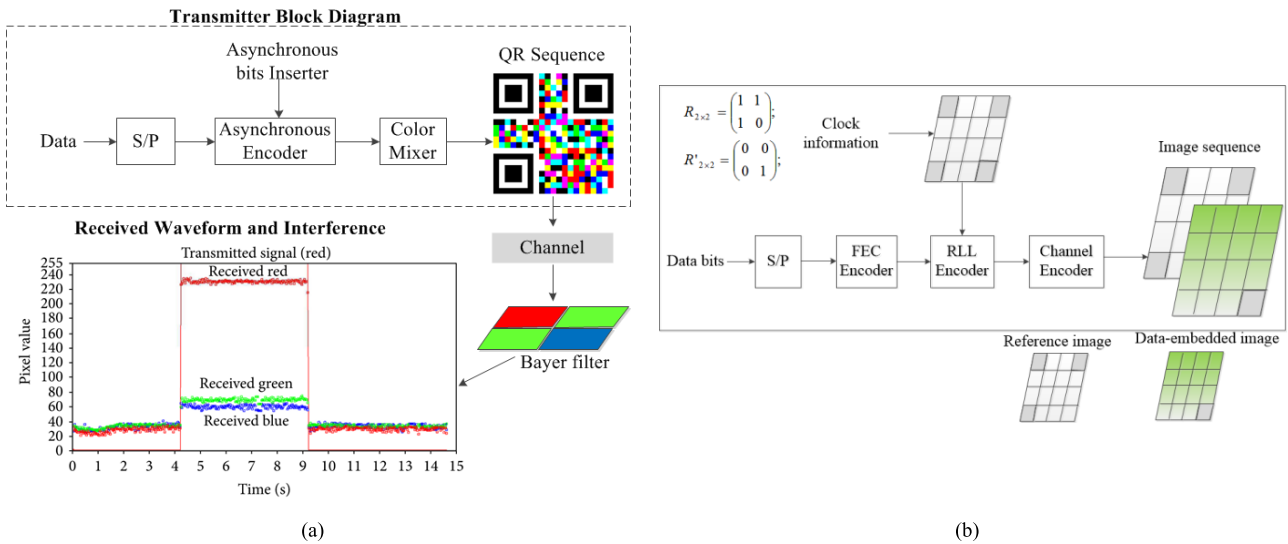
FIGURE 4. Screen modulation reference architecture. (a) 2D sequential color code. (b) 2D hidden Code with differential coding.

considered, including frame rate, exposure (i.e. light integration time), row sampling rate (especially for rolling shutter camera) and image resolution. Communication-related performance is the foremost priority, whereas variations in the parameters that lead to the need for image-sensor compatibility are secondary.

For the communication performance, along with the need for typical image-sensor compatibility, we must identify parameters that mainly limit the communication bandwidth. The frame rate (or row sampling rate, especially in the rolling-shutter camera Rx) that varies slightly or considerably is the limit for the optical clock rate of transmission at the Tx, satisfying the Nyquist sampling rate, whereas the long exposure time, which is controlled by the "Integrate & Hold" block, takes a role as the low-pass filter, limiting the upper threshold of the communication bandwidth to typically less than tens of kHz. Moreover, the resolution of the image allows the Rx to receive signals from multiple light sources simultaneously, performing the visual MIMO technique.

B. E_b/N_0 CALCULATION
Based on the model of image sensor, the pixel E_b/N_o is estimated [34] as follows

$$Pixel \frac{\in_b}{N_0} = \frac{E[s^2]}{E[n^2]} \approx \frac{a^2 \Delta}{\alpha a \Delta + \beta} \qquad (1)$$

where E_b represents the Energy-per-bit; N_0 represents the Spectral-Noise-Density; s is the pixel value; a is the amplitude of the signal; Δ is the camera exposure duration as a ratio of the signal cycle; $\Delta = t_e/T$; n is noise value $n \approx N(0, \alpha(s)^2)$; α, β are noise model fit parameters.

The calculation of the pixel E_b/N_0 ratio in our OCC system differs fundamentally from the typical calculation of E_b/N_0 in an RF system. The difference between the Rx of an RF system and Rx of our OCC system derives originates from

the image sensor Rx and its mechanism of exposure to light intensity. A camera Rx is solely based on what the image sensor detector sees within the integration time, *i.e.*, from the time the shutter is open to the time it is closed. The shutter speed relates to the integration time that is simply a fraction of the bit interval (*i.e.*, multiple times less than 1%), and the following relationship between the error probability and pixel E_b/N_0 shall be unfamiliar to the RF system.

The fit parameters $\alpha = 0.01529$, $\beta = 0.1973$ introduced in [34] are used. For our intended systems, two options of the shutter speed at 1and 8 kHz are provided to compare, and the optical clock rate of Tx at 125 Hz is selected. From these values, we obtain the relationship between the pixel amplitude and E_b/N_0, as shown in Fig. 3(b). The estimation shows that the curve is not linear. Even when a signal is absent, residual noise power may still exist. Moreover, a very high pixel E_b/N_0 can be achieved when the pixel amplitude acquired is close to the maximum value, such as 255 for 8-bit ADC pixel. Notably, compared with a lower shutter speed (e.g., 1 kHz), a faster shutter speed (e.g., 8 kHz) shall require a lower bit energy to attain the desired pixel amplitude. The estimation of bit energy as a function of pixel amplitude is useful in practically measuring and estimating the performance of OCC systems.

IV. SCREEN BASED NYQUIST SAMPLING
A. REFERENCE ARCHITECTURE
The pervasive use of screens can be viewed as communicating a 2D code to camera-equipped sensors. Two types of screen modulation are introduced in Fig. 4 based on their perceptibility characteristic of modulation to human eyes: (i) color modulation, shown in Fig. 4(a), and (ii) hidden modulation, shown in Fig 4(b). Color modulation attracts users by informing where the transmitter is. In contrast, hidden code objects protect data from any unintended attention.

Both types of screen modulation shall implement multiple cells simultaneously transmitting data to multiple pixels of the image sensor to achieve the desired data rate. The modulated light coming to the image sensor is filtered by Bayer RGB filter. Thus the interference between R, G, and B color channel is present in our color transmission system. Numerous studies [15]–[21] have investigated the types of color modulation in the space-time domain. On the other hand, the modulation in the grey channel or watermarking is highly affected by the ambient light. Thus line coding is used in conjunction with channel coding to enhance the performance of hidden code systems. Also, numerous studies [22]–[24] have investigated the hidden-cell modulation.

Supporting the operation under camera rotation and under the rolling shutter effect, a principle of clock information embedded into four corners of the code is introduced as Fig 4(b) showed.

B. PERFORMANCE EVALUATION

According to A. Ashok *et al.* [59], the capacity of space-time modulation can be expressed using Shannon Capacity formula, considering the deterministic nature of perspective distortions and the AWGN characteristic of the camera channel:

$$C = F_{fps}(W_s \log_2(1 + SINR)) \tag{2}$$

where SINR represents the signal-to-interference-noise ratio per pixel, F_{fps} is the camera-frame rate, W_s is the spatial-bandwidth, which denotes the number of information carrying pixels per camera image frame. The spatial bandwidth is equivalent to the number of orthogonal or parallel channels in a MIMO system.

The calculation of SINR under presence of perspective distortion is also provided as

$$SINR = \frac{\alpha P_{avg}^2}{(1 - \alpha)P_{avg}^2 + \sigma_n^2} \tag{3}$$

where P_{avg} denotes the average transmit pixel intensity. The average perspective distortion factor $\alpha (0 \leq \alpha \leq 1)$ represents how the signal energy on each pixel is effective area scaling (down) due to perspective and lens-blur in the camera imaging process, while the rest of the light-energy on the pixel is from ambient photon noise. $\alpha = 1$ indicates that the screen pixel is at the focus of the camera and also incurs no signal reduction due to lens-blur, and $\alpha = 0$ indicates that no part of the screen-pixel gets imaged on the camera pixel.

To deal with a high perspective distortion in which the interference between pixels happens, a channel block coding in the space domain [15], [16], [20], may be applied. A block of β pixels that may interfere with each other shall be used to map some bits. In this case, the SINR that indicates the signal-to-interference-noise ratio of the entire block is used.

$$SINR_{blk}(\alpha, B) = \gamma_1 SINR_\alpha + \gamma_2 SINR_\alpha \quad \forall \alpha\beta > 4$$
$$= SINR_\alpha \quad \forall \alpha\beta \leq 4 \tag{4}$$

where $SINR_\alpha$ is calculated from (3), the coefficient $\gamma_1 = 4(\sqrt{\alpha\beta} - 1)$ and $\gamma_2 = (\sqrt{\alpha\beta} - 2)^2$ represent the number of boundary-blocks and non-boundary blocks respectively. Here min $\beta = 4$ (i.e. 2×2 pixels), and $\alpha\beta = 4$ indicates that each β pixel block projects onto a maximum of 1 camera pixel area while $\alpha\beta > 4$ indicates that the block project onto multiple camera pixels.

For hidden code series, due to the low signal-to-interference-noise ratio, line coding shall be applied. A popular way to deal with the noisy channel is to use a differential coding, which uses two adjacent images to map a block of data bits. The dissimilarity of two adjacent sampled frames is objected to decode a block of data bits. Pixel-based metric, calculates the difference of the pixel color intensity values of the two frames [62]. For frames F and F' each with $X \times Y$ pixels, the pixel-based matric $d_p(F, F')$ is calculated as:

$$d_p(F, F') = \frac{\sum_{\substack{1 \leq i \leq X \\ 1 \leq j \leq Y}} |C(p_{ij}) - C(P'_{ij})|}{X \times Y} \tag{5}$$

where $C(p_{ij})$ and $C(p'_{ij})$ are the color intensity values of pixels p_{ij} and p'_{ij} in frame F and F', respectively.

Based on the differential pixel-based matrix, the calculation of SINR is performed using (3), determining the maximum capacity of a system like (2) showed.

From the implementation view, the performances of highlighted systems are compared. Fig. 5(a) shows normalized communication parameters of the selective modulation schemes. It shows the comparison of Tx resolution and Tx clock rate (Hz) among the modulation schemes. In Fig. 5(b), throughput values of different screen-camera modulation schemes has shown.

PixNet system developed by S.D. Perli *et al.* [15] encodes data in the frequency domain by adopting a 2D OFDM modulation scheme. The main components of PixNet include a perspective correction algorithm, blur-adaptive OFDM coding, and an ambient light ?lter. The throughput reaches multiple Mbps; however, the slow processing time causes to a low optical clock rate of transmission (no more than 5Hz, i.e. five blocks are transmitted per second). COBRA developed by T.Hao *et al.* [16] uses a new 2D color barcode design that is particularly optimized for real-time streaming between small-size screens and low-speed cameras of smartphones. Five colors including black, white, red, green, and blue are used. Three optional colors including magenta, cyan, and yellow may also be used. The 10Hz data block transmission provides the reliable link. The throughput performance depends significantly on what the Rx device is used.

V. HIGH FRAME-RATE NYQUIST SAMPLING
A. REFERENCE ARCHITECTURE

Unlike the modulation of screen light which operates at a low frequency (i.e. less than 20Hz) being less intrusive to the human eye, herein and following sections, the primary illumination purpose of LED light sources leads to the requirement
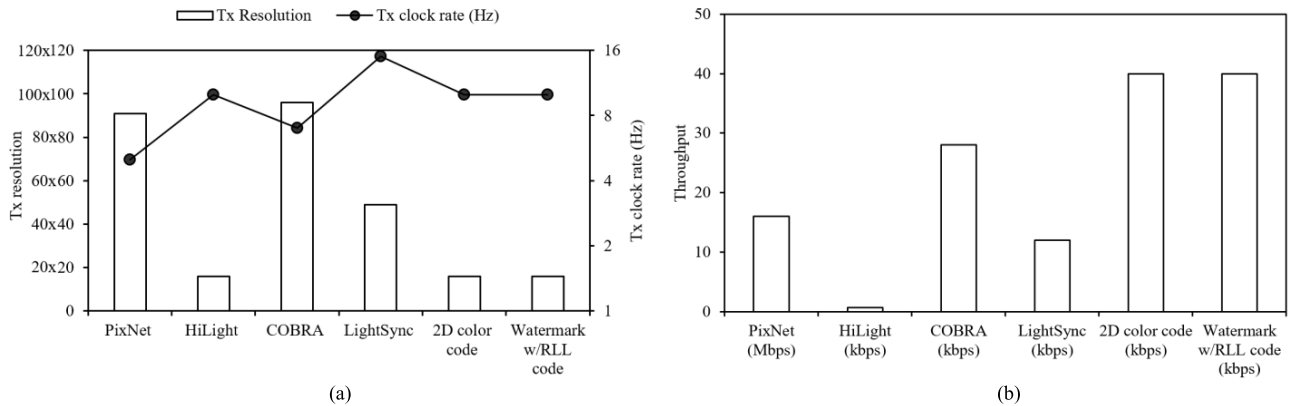
FIGURE 5. Performance comparison between screen modulations. (a) Normalized communication parameters. (b) Throughput value of selected screen modulation.
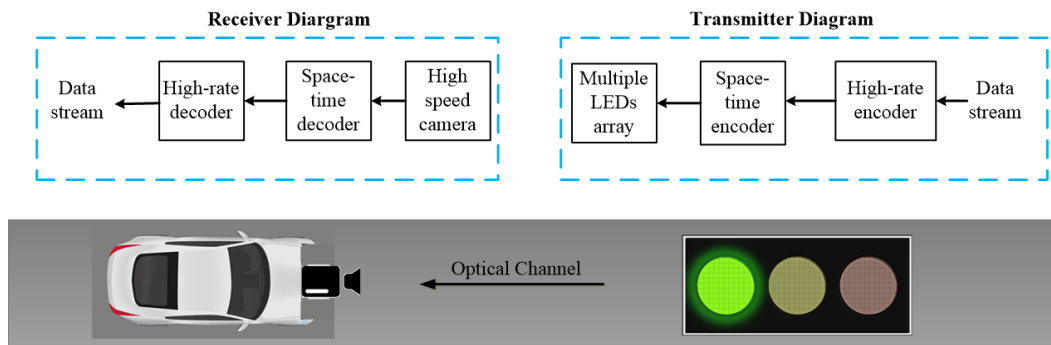

FIGURE 6. Infrastructure-to-vehicular reference architecture using traffic lights and high-speed camera.

of flicker-free modulation. The optical clock rate to drive LED light sources is at a higher frequency (i.e. greater than 100Hz [54]). The oversampling technique means that the camera sampling rate (i.e. frame rate) is multiple times higher than the optical clock rate. Consequently, the frame rate of the camera is kfps or even higher. The reference architecture is shown in Fig. 6.

High-speed cameras can simply handle the demodulation of hundred(s) Hz modulated light by taking their advantage in the oversampling ratio between the frame rate of Rx and the clock rate of Tx. Nonetheless, the use of high-speed cameras is an ineffective cost solution for some services. Undeniably, a typical camera at a low frame rate (such as 30fps) is inapplicable to those protocols. Multiple-LEDs array shall be used to implement the space-time coding series to apply the optical MIMO concept. It has been shown that the schemes apply to the vehicular environment at which light sources are available on cars or traffic lights, traffic signs and high speed cameras are equipped in cars or traffic CCTV systems.

The studies on space-time coding for high frame-rate Nyquist sampling optical system are various [27]–[32]. The dimming support trend is greatly affected to the illumination device; however, to the best of our knowledge, we have not found a research related to dimming support for those related systems. It may be acceptable in using traffic light at

this time while the traffic light source is turned on and off at a time without any dimming requirement.

B. PERFORMANCE OF FRAME RATE OVERSAMPLING
For example of a high-speed camera based transmission protocol presented in [27], it uses an A-On-A'-Off protocol with all beacon data repeated n-times (where A' is the inverse form of a block of data A). Similarity, a space-time code (Space Shift Keying) generating two blocks of 2×2 LED matrix to transmit 2 data bits is proposed by Katsunori *et al.* [28]. The authors used a 1000 fps vehicular camera. Later, an updated protocol for $2^n \times 2^n$ LED matrix namely the Layered Space-Time Code was proposed by the authors to deal with multiple LEDs and data rate adaption against distance [30]. A high-speed camera based OCC with the less oversampling ratio of 3/2 emanates from our previous study [29] in which the camera frame rate is assumed to be constant.

The tradeoff between diversity and multiplexing gain is considered in any space-time coding system, and OCC system is not an exception. Implementing visual MIMO concept, OCC systems gain a low spatial multiplexing gain as shown in Fig. 7(a). However, this is not a problem because the current resolutions of the image allow a large amount of simultaneous data streams over LOS links. Several studies have proposed the method to embed multiple data streams
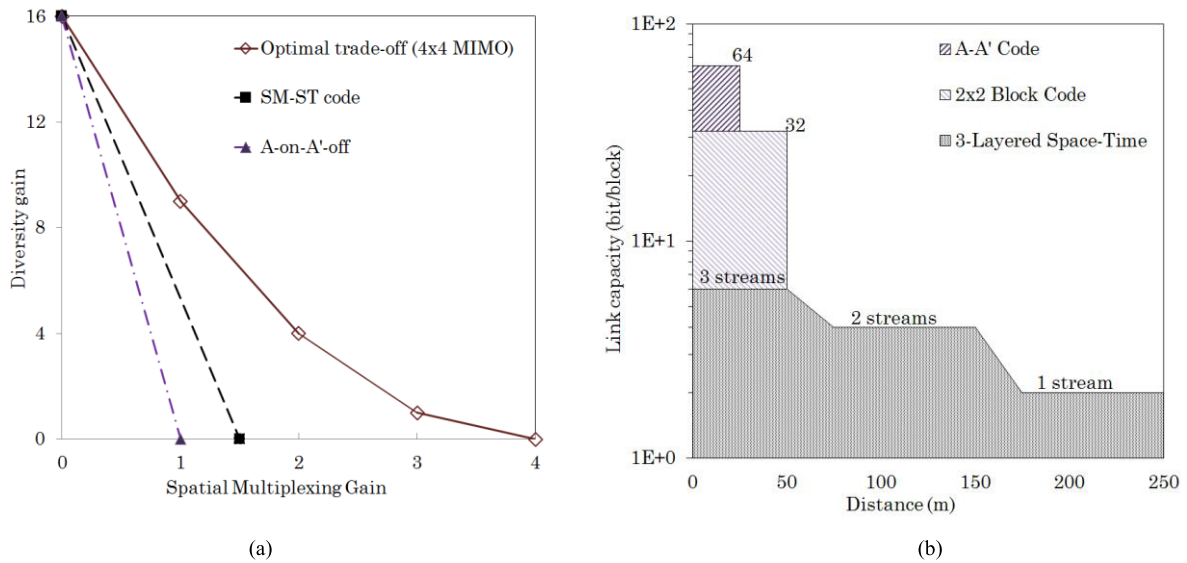
FIGURE 7. Performance comparison between high-frame-rate Nyquist sampling techniques. (a) Diversity-multiplexing tradeoff for high frame-rate processing Space-time codes (4 LEDs Tx). (b) Link capacity against distance.
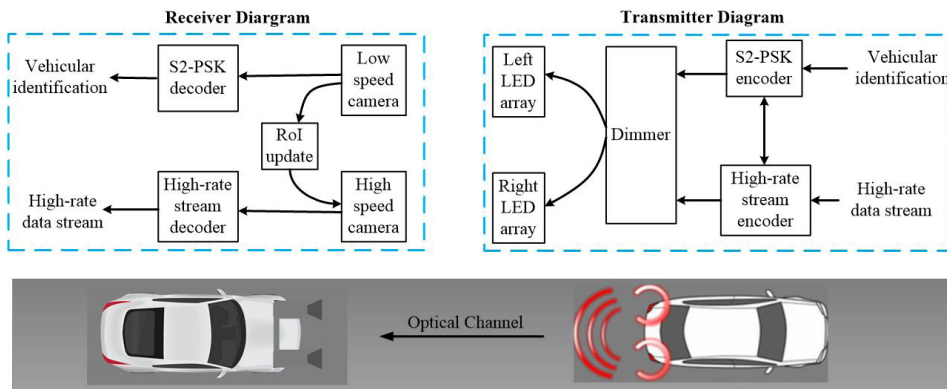

FIGURE 8. Reference architecture for RoI signaling system employing S2-PSK.

by using the same multiple LEDs Tx to deliver different data stream according to the distance from Tx to Rx. Fig. 7(b) illustrates the link capacity of different data streams against distance. The distance adaption is beneficial from the spatial separation characteristic of LOS links via OCC.

VI. UNDERSAMPLED ROI SIGNALING

A. REFERENCE ARCHITECTURE

The unmitigated matter of oversampling technique presented in the previous section concerns about the requirement of a high-speed camera. The camera Rx that requires maintaining its frame rate at high speed whereas the heavy processing involved in the detection of light source transmitter(s) and demodulation of data is unavoidable.

The scheme, therefore, is cost-ineffective. Fortunately, the RoI technique that is familiar to camera developer is suitable for camera Rx to achieve high frame rate while minimizing the computational cost in the light source(s) detection

and extraction. Herein, the methodology of implementing RoI based communication is discussed. The architecture for RoI signaling is illustrated in Fig. 8.

The transmission of RoI is beneficial when the camera Rx knows the area in which the communication link should be setup. The light source Tx shall continuously inform the camera Rx via a known signal for differentiating the light source Tx from other non-interested light sources and other objects. The transmission of the known signal is a type of light source identification. Moreover, the high-speed data stream is embedded into the low-speed RoI stream. A dual streaming of light source identification signaling and high-speed data link is performed as the hybrid modulation.

For the Rx, light source identification and demodulation of high-speed data can be time slotted using a single camera. This means that the camera Rx first detects the RoI from the light source identification signal, and then selects the RoI to accelerate the frame rate and achieve high-speed data link.
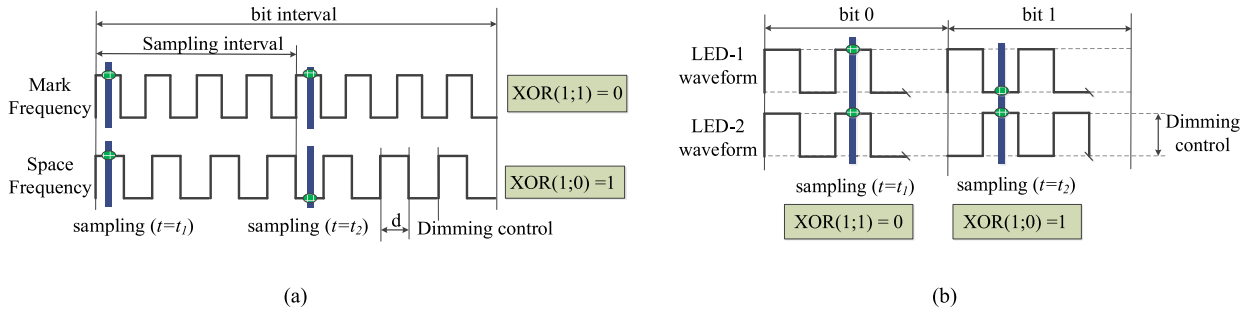
FIGURE 9. RoI signaling waveforms. (a) UFSOOK waveform. (b) S2-PSK waveform.

However, the movement between Tx and Rx is considered and the RoI may also move. The alternative solution is the use of a dual-camera system in which one camera simultaneously detects the RoI for another camera that is demodulating data at high-speed. The low frame-rate (e.g. 30fps) camera shall be used to detect the RoI to reduce cost.

Different RoI waveforms are compared in Fig. 9. The UFSOOK waveform is undersampled in the time domain, and multi-phases used to correct the error under dimming. Conversely, the S2-PSK waveform is undersampled in the spatial domain, and amplitude modulation is used to control the dimming.

B. PERFORMANCE OF UNDERSAMPLING AND RoI TECHNIQUES

Assume that the probability of a wrong decision for bit 1 (transmitted 0 bit decided 1) and bit 0 (transmitted 1 but decided 0) is the same bit error rate. For a temporal scheme of undersampling such as UPSOOK, assume that the sampling #n and sampling #(n+1) are independent, the overall error probability of the XOR operator is estimated as

$$P_{e,temporal\ undersampled} = p(s_{1,decoded}$$
$$= correct, s_{2,decoded} = false)$$
$$+ p(s_{1,decoded} = false, s_{2,decoded} = correct) \quad (6)$$
$$P_{e,temporal\ undersampled} = 2p_e(1 - p_e) \quad (7)$$

where p_e is the error probability of the LED state decision of 2-PSK in UPSOOK, and that of 2-FSK in UFSOOK.

Unlike the temporal scheme, our spatial scheme S2-PSK demodulates a bit from a pair of states (two states of two different LEDs) from the same image. Similar to UPSOOK, a wrong demodulation solely occurs when one state among those two is improperly decided while another is correctly decided. However, given that those two states are from the same image, hence there is a high similarity in the noise experienced. Considering a suitable method of noise mitigation for the decoding, the demodulation within an image can gain a lower bit error rate compared with UPSOOK. This noise can be mitigated by using the nonlinear XOR classifier with a suitable intelligent algorithm (e.g. Artificial Neural Network (ANN) for exclusive-OR (XOR) operator proposed in [38]). Overall, the error probability in classifying on and off states of light sources is enhanced substantially with the XOR decoder, and the BER performance of the S2-PSK scheme is

expressed as:

$$P_{e,S2-PSK} = 2\alpha p_e(1 - \alpha p_e) \quad (8)$$

where (αp_e) is the error probability of LED state performed by the nonlinear XOR classifier; $\alpha < 1$ is the error rate enhancement coefficient achieved by using the XOR classifier.

Fig. 10 presents the BER performances of the RoI signaling techniques without or with various dimming level. A comparison of BER against $\varepsilon b/No$ performance for the different schemes shown in Fig. 10(a) is performed over the simulations without dimming (i.e., the average brightness was kept constant at 50%). Here, the energy (per bit) required by UPSOOK was lower than that required by UFSOOK to achieve the same bit error rate. S2-PSK showed a lower bit error rate than UPSOOK at the same noise level, because the bit demodulator (XOR operator) could mitigate the similar noise that appears in a pair of input states within the same image.

The BER performance may change under dimming (brighter or darker) as illustrated in Fig. 10(b). Since UFSOOK performs dimming via duty cycle modulation whereas UPSOOK and S2-PSK use AM, UFSOOK maintained its performance while that of the other two techniques was compromised. As can be seen, UFSOOK can maintain the performance with multi-phase sampling (such as a 3-times repeating (R3) code) is applied to correct the sampling error. However, when scarifying the data rate for repeating code, UFSOOK provides better performance than S2-PSK dimmed at 25%. Fortunately, the simulation and calculation of pixel Eb/No in Section III(B) show that a light-of-sight link greater than 20dB E_b/N_o is fully achievable with the current shutter speed. Moreover, the ANN approach works well with nonlinear classification matter in the XOR function of the S2-PSK system, ensuring that OCC systems work well under lower dimming.

C. HIGH-SPEED DATA STREAMING VIA SELECTED RoI
1) TWINKLE VPPM
The UFSOOK sends the information for the light source and RoI identification. Along with the low-speed amplitude change, the actual data rate that a high-speed camera demodulates is based on the rapid change of the VPPM clock
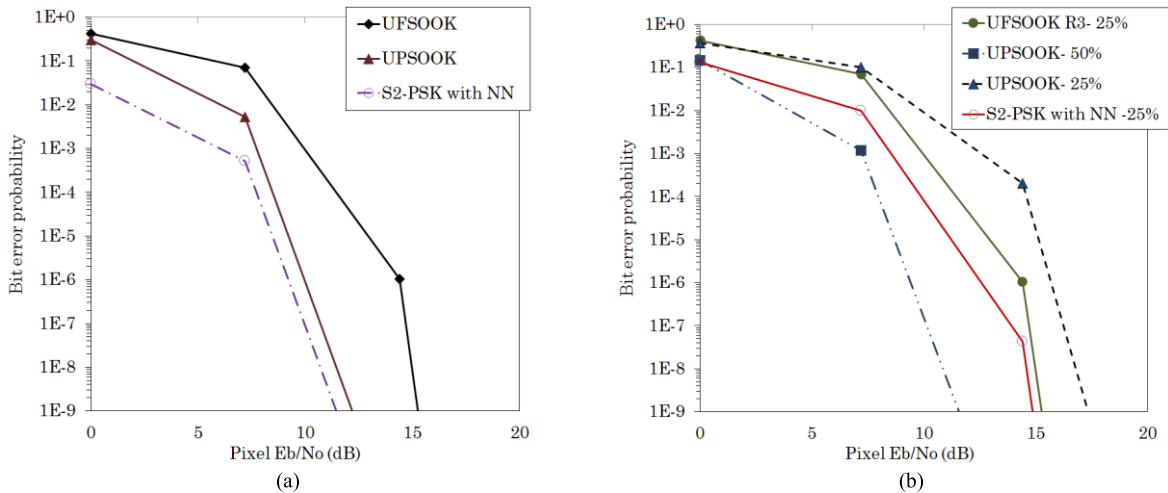
FIGURE 10. BER against *Eb/No* curves of RoI signaling techniques. (a) BER against pixel *Eb/No* curvers of undersampling modulations (without dimming). (b) BER against pixel *Eb/No* curvers of undersampling modulations (under dimming).
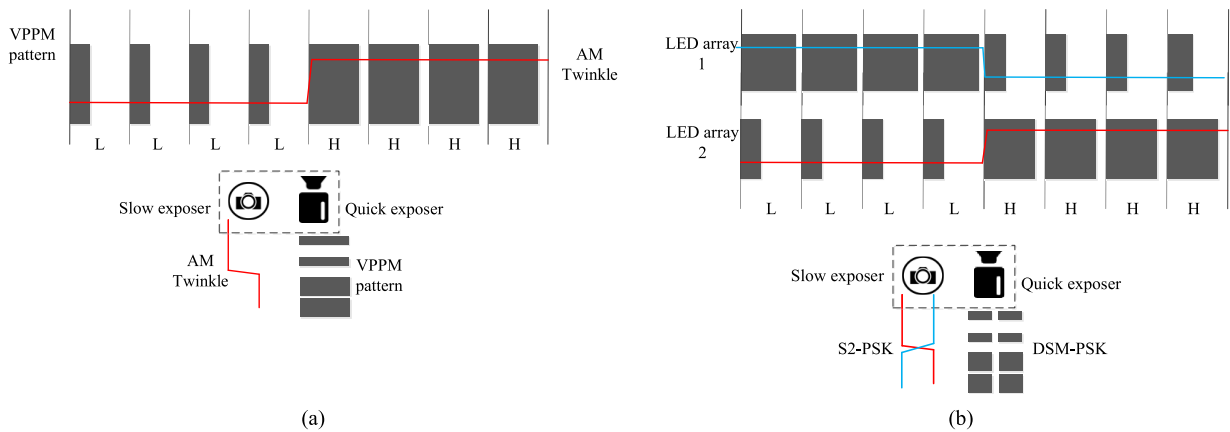

FIGURE 11. Dual data streams generation in RoI based OCC systems. (a) Dimmed Twinkle VPPM waveform generating UFSOOK signal. (b) Dimmed Hybrid S-PSK waveform generating S2-PSK signal.

rate. The hybrid modulation of the AM change and the VPPM is called twinkle-VPPM. The twinkle VPPM waveform generation is illustrated in Fig 11(a).

Two cameras observe the pulsating light. The first camera has a fast exposure such that it can decode the high pulse rate (the high-speed camera). The second camera has a slow exposure time such that it only perceives light with constant intensity (the 30 fps camera).

The demodulation is a Nyquist sampled communications that considers the communications to be quasi-synchronous. Specifically, the AM twinkle frequency is at 127.5Hz to target the frequency equaling (n ±1/4) times the frame rate, where n is a selected integer. Using 4 samples per AM cycle, the aliased twinkle frequency guarantees the AM demodulation even if every other sample falls on a transition boundary. The bit rate of AM is 7.5 Hz.

2) HS-PSK

The modulation is specialized for vehicular application in which a pair of light sources (a pair of tail light or a pair of the headlight) is to transmit data. The HS-PSK waveform

generation is illustrated in Fig 11(b). The DSM-PSK evenly dims the light sources at the low and high dimming levels, which generates an AM signal at a low frequency of 200Hz (or 125Hz). The AM signal is modulated following the encoding rule of the S2-PSK. The bit rate for the AM signal is usually 10Hz; therefore, it supports any camera with the frame rate at no less than 20fps for successfully demodulating the AM signal. The random sampling of the camera is considered; hence the communication is totally asynchronous. At the initial state of TG7m standardization, a high-speed data link up to 22 kbps generated by HS-PSK is introduced for vehicular communication purposes.

VII. HYBRID OCC AND PD COMMUNICATION
A. REFERENCE ARCHITECTURE
There are variations between the related works on hybrid OCC and PD systems realizing a new type of image sensor comprising PD cells (communication cells) integrated between image pixels (image cells). The image output from the image cells is used to detect the light source; then a communication link is set up and the PD cells are activated.
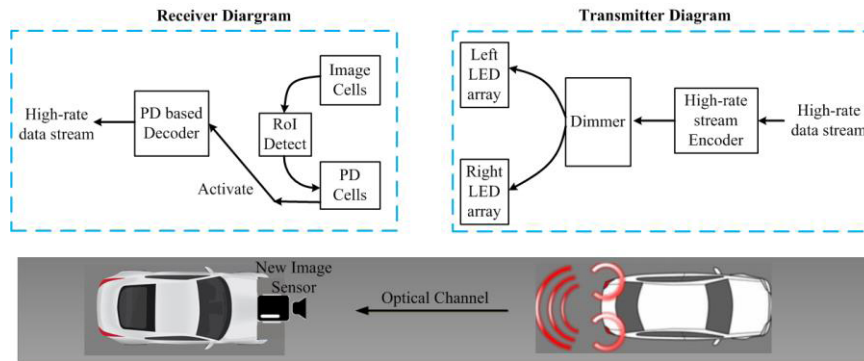
FIGURE 12. Reference architecture for Hybrid OCC/PD communication system based on RoI signaling technique.
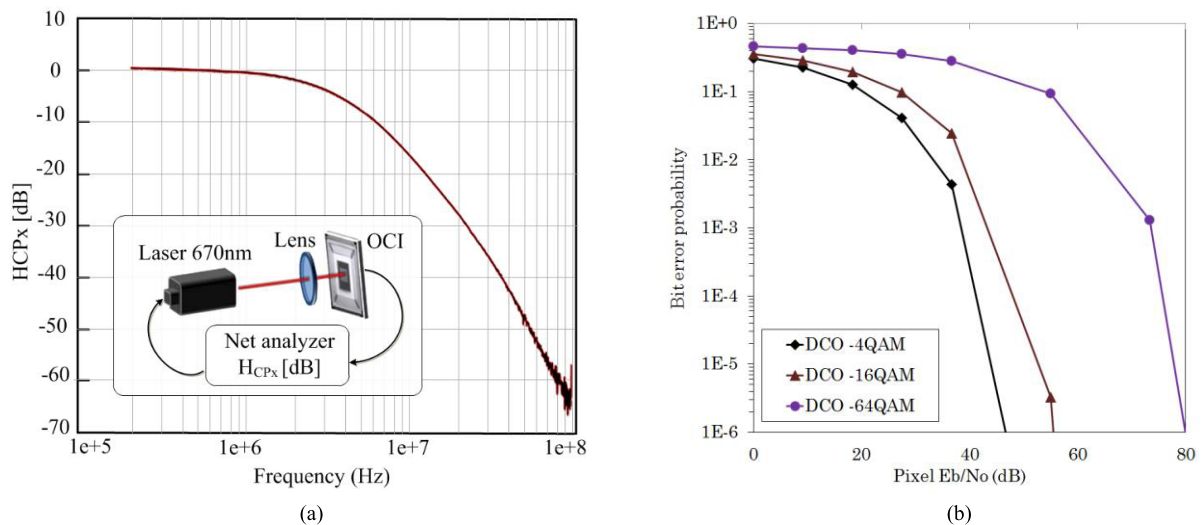

(a)

(b)

FIGURE 13. Operation and performance of Hybrid OCC/PD systems. (a) Measurement of frequency response characteristics (redrawn from [40]). (b) Simulation result of bit error rate against pixel Eb/No for PD communication in hybrid system (re-simulated from [42]).

The technique also requires the detection of RoI; however, RoI signaling is missing, and Computer Vision based RoI detection is performed instead. The reference architecture for hybrid OCC/PD system is shown in Fig. 12.

B. PERFORMANCE EVALUATION

To the best of our knowledge, most of the related works did not evaluate the performance of RoI detection because the detection of the light source is solely based on image processing. The detection of the light source without the RoI informing functionality, similar to the case of previous Undersampled RoI signaling technique, is problematic. The evaluation of RoI detection using the computer vision technique and the undersampled-RoI signaling technique has been presented in our previous work [38], which reports the outstanding performance of the RoI signaling technique at large car-to-car distances.

Assume that the RoI is successfully detected, and communication pixel (CPx) is PD-activated according to the detected RoI from image cells. After this link setup step, the performance of high-rate link is based on the performance of PD and its circuit (such as an equalizer). The frequency response of communication pixel (HCPx) experimentally

measured [40] is shown in Fig. 13(a). The frequency response allowed the occupied bandwidth up to 10MHz with the equalizer considered.

After the bandwidth is selected, the proper modulation may produce a desired performance. Typical modulation schemes such as OOK and VPPM standardized by IEEE 802.15.7-2011 standard are useful. However, advanced modulation and coding schemes for optical wireless communication, such as OFDM series, present new opportunities for our hybrid OCC and PD communication system.

Fig. 13(b) illustrates the bit-error rate as a function of the E_b/N_o performance of direct current-biased OFDM (DCO–OFMD) using quadrature amplitude modulation (QAM) symbol mapping. It shows that 10^{-6} BER shall require the signal strength above 40dB (up to 80 dB). Fortunately, from our experiment, the line-of-sight link satisfies the required signal strength realized by vehicular light sources at a reasonable distance (such as 100m or greater).

VIII. ROLLING SHUTTER SAMPLING

A. REFERENCE ARCHITECTURE

In addition, related to flicker-free modulation, a rolling shutter camera based OCC systems [44], [45], [53] can take
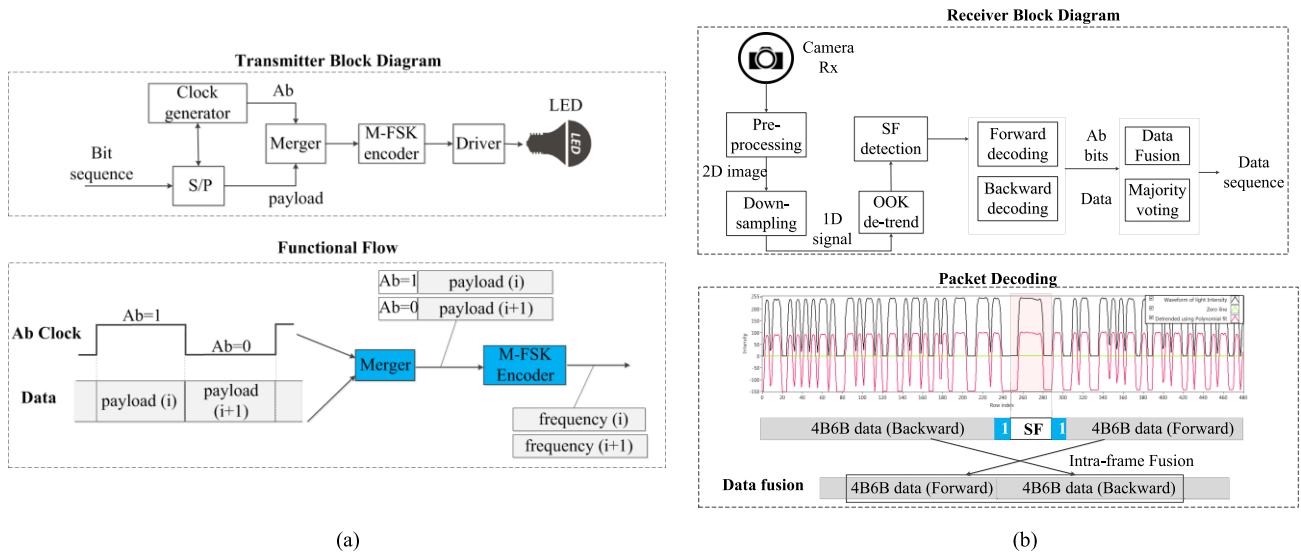
FIGURE 14. Reference architecture for rolling shutter based OCC systems. (a) Rolling shutter OCC reference architecture employing CM-FSK. (b) Rolling shutter OCC reference architecture employing OOK.

advantage of the rolling shutter mechanism which sequentially exposes pixel lines to the incoming light.

Fig. 14 illustrates two promising approaches of rolling shutter sampling based on highlighted works listed in Table 2. Fig. 14(a) presents a block diagram of the CM-FSK system [52] proposed by Kookmin University. Compared with a similar M-FSK proposed by Carnegie Mellon University [49], CM-FSK is designed to embed the clock information into every single frequency symbol to support varying-frame-rate cameras. Also, in functional blocks, it is similar to the RS-FSK system developed by National Taiwan University [50]. The major difference between the RS-FSK system and two other systems is the frequency separation. M-FSK and CM-FSK maintain the frequency separation at a constant value, while RS-FSK keeps the inverse value of the frequency separation at a constant.

Fig. 14(b) presents an example of rolling shutter sampling OCC system in the time domain, employing OOK modulation. Packet PWM/PPM from Panasonic [47], [48] is also a type of temporal rolling shutter camera sampling. Here in the exemplary system, we highlight the importance of a technique called data fusion which merges data from multiple images to support the reception of a longer packet at a distance.

Dimming is crucial to the modulation, and the PWM/PPM code by Panasonic supports the best dimming. The modulation pulse width in steps of 60 micro sec [48] allows the best dimming control; however, it is designed for cameras that have a higher bandwidth capacity (i.e. 16 kHz bandwidth). The smallest pulse width of 10 micro sec shall require 200 kHz sampling rate of an image sensor Rx, a requirement that most of current smartphone cameras cannot reach.

Finally, the hybrid modulation of M-FSK and 2-PSK is designed to support larger distances (up to 20m via

2-PSK link) [52] while maintaining the advantages of M-FSK, including the power efficiency and the image sensors compatibility support.

All the rolling shutter sampling OCC systems encounter the same problem of distance limitations and data rate limitations owing to the operation of the rolling shutter mechanism. Details on the performance comparison between different schemes reaching to the limitations of data rates and distance are analyzed in the following sections.

B. DATA RATE - DISTANCE TRADEOFF

Given the operation of the rolling shutter camera, the actual number of samples (pixel rows) acquired from the captured image of the light source at distance d, $N_{row}(d)$, is calculated as.

$$N_{row}(d) = w \frac{L/(2 \tan(\frac{FOV}{2}))}{d} \qquad (9)$$

where w is the image width (in case the rolling axis is along the width of the image sensor), L is the normalized length (diameter) of the light source along the width of the image sensor, d is the distance between the light source Tx and the camera Rx, and FOV is the field of view of the camera.

The actual number samples acquired from an image, $N_{row}(d)$, determines the amount of information that an image can capture. Two different approaches of demodulation, frequency domain and time domain based demodulations are described as follows.

1) PERFORMANCE LIMITATION OF FREQUENCY DEMODULATION

The sampling rate of the image sensor, which is the frequency at which a row of pixels is sampled, must be at least twice the rate of the highest signal frequency, according to Nyquist's theorem. This relationship is described by the
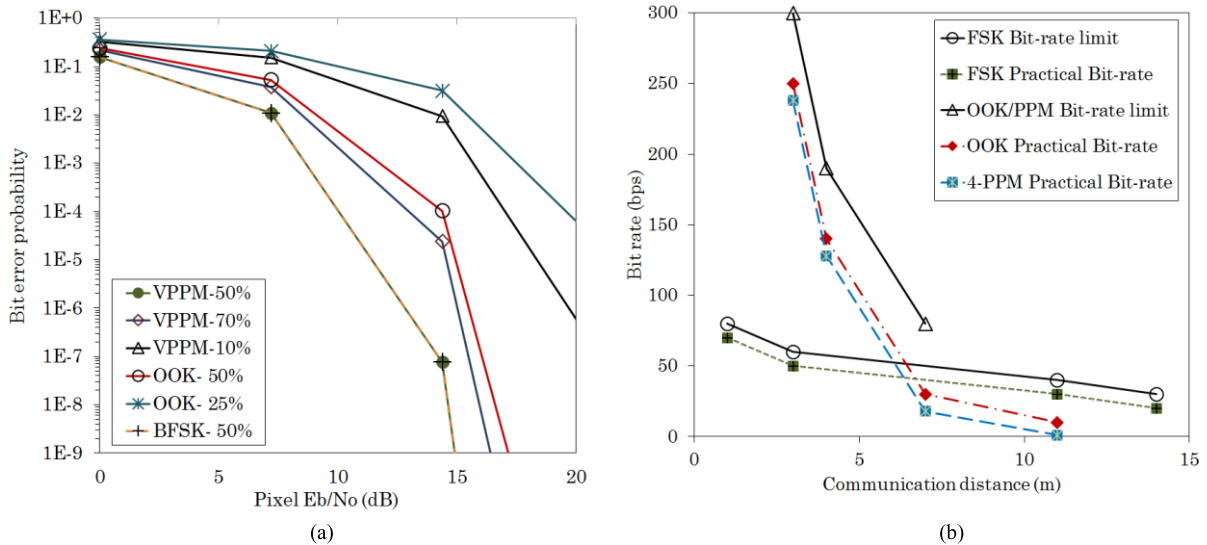
FIGURE 15. Performance of rolling shutter based OCC systems. (a) BER against *Eb/No* curves of rolling shutter sampling techniques. (b) Link capacity of rolling shutter OCC modes versus distance.

following equation:

$$f_{\max} = f_{Nyquist} = \frac{f_s}{2} \tag{10}$$

where f_{max} is the maximum resolvable frequency, $f_{Nyquist}$ is the Nyquist frequency, and f_s is the sampling rate of the image sensor (i.e., the sampling rate of lines of pixel).

The frequency resolution (Δf) is dictated by the acquisition time and given as

$$\Delta f = \frac{1}{T} = \frac{f_s}{N_{row}(d)} \tag{11}$$

where T is the acquisition time (of a rolling image), N_{row} is the number of samples (i.e., lines of pixel) acquired throughout the diameter of the light source along the rolling direction of the image sensor.

From (10) and (11), the condition for the camera Rx to differentiate a frequency is that the size of the light source on the captured image is large enough, namely,

$$N_{row}(d) \geq \frac{f_s}{\Delta f} \tag{12}$$

From (8) and (12), the requirement of the light source size on the captured image leads to the upper-limited communication distance, which can be computed as follows

$$d \leq \frac{(\Delta f)w}{f_s}(L/(2\tan(\frac{FOV}{2}))) \tag{13}$$

From (13), the maximum distance of transmission is proportional to the frequency resolution and the size (diameter) of the light source.

2) PERFORMANCE LIMIT OF TEMPORAL DEMODULATION

Unlike FSK, wherein a single frequency symbol is demodulated per image, OOK or Packet PWM/PPM systems demodulate the entire packet including multiple symbols per image. Thus the size of data sub-packet shall be short enough to be

captured entirely by an image in the case where data fusion technique is not applied. The conditional size of the light source on the captured image is expressed as

$$N_{row}(d) \geq 2f_s T_{sub\_packet} = 2f_s/R_{DS} \tag{14}$$

where R_{DS} is the data sub-packet rate, and T_{sub_packet} is the length in time of the data sub-packet.

Consequently, from (8) and (14), the communication distance is limited as a function of the data sub-packet size as follows:

$$d \leq \frac{w \times R_{DS}}{f_s} \times (L/(4\tan(\frac{FOV}{2}))) \tag{15}$$

Moreover, besides the distance limitation which is linearly proportional to the data sub-packet length as shown in (15), the temporal rolling shutter decoder shall require the number of samples to clearly differentiate between the on and off states of the captured waveform in the time domain. A minimum of four samples per clock is suggested to identify whether the transmitted state during the clock time is on or off. The condition is expressed as,

$$f_s T_{sub\_packet} = f_s/R_{DS} \geq 4N_{B/sub\_packet} \tag{16}$$

where N_{B/sub_packet} is the number of binary clocks per data sub-packet.

Fig. 15(a) presents the simulated bit error rate against pixel E_b/N_o performance of the OCC systems employing OOK, VPPM, and FSK with various dimming levels. We applied pulse width control for VPPM and FSK dimming; however, we applied the amplitude control for OOK dimming as it is suitable for an OCC system. Undeniably, Binary FSK (BFSK) shows the best performance because it requires the lowest pixel E_b/N_o to achieve the desired BER. VPPM outperforms under dimming. VPPM dimmed at 10% provided a better performance than OOK dimmed at 25%. This is because the amplitude dimming control is applied for OOK
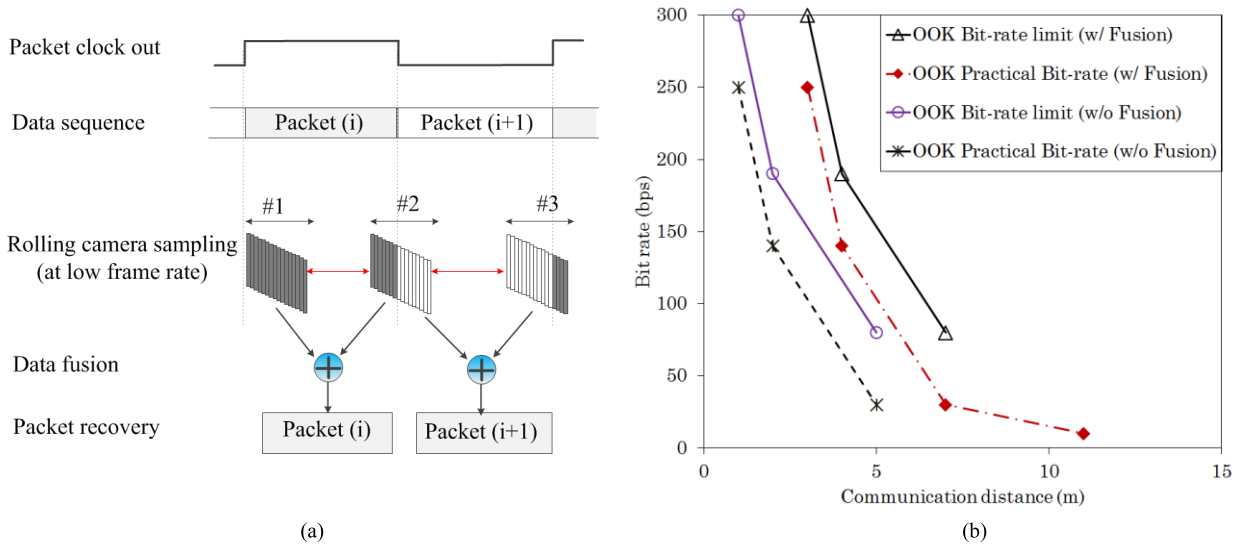
FIGURE 16. Performance enhancement of packet fusion technique for rolling shutter OCC. (a) Data fusion technique to recover a longer-length symbol from multiple images. (b) Distance Improvement using the packet-fusion technique.

to maintain the link rate. Fortunately, our experiment of pixel intensity along with the calculation of pixel E_b/N_o in Section III-(B) always guarantee the pixel E_b/N_o at greater than 30dB for the light-of-sight link at an intended indoor distance such as 10 m, ensuring that the OCC systems perform well under low dimming.

Fig. 15(b) displays the bit rate against distance performances of OOK, VPPM, and FSK modulation schemes. Temporal modulation series (including VPPM and OOK) provide higher bit rates at the same distance compared to frequency modulation series (such as RS-FSK and CM-FSK). However, for the communication distance, the OOK scheme cannot extend the communication as much as FSK can. (13) and (15) describe the calculation of the maximum distances of all those schemes. The trade-off between the distance coverage and the data rate suggests the selection of a proper modulation for the intended system.

C. DISTANCE IMPROVEMENT OVER DATA FRAME FORMAT
To extend the maximum distance of communication, a fusion technique has been proposed [46] in which the sub-packet is merged from two adjacent images using asynchronous bits (Ab). This sub-packet is decodable if every image captures no less than half of the data sub-packet size. Hence, the size of the image allowed is two times smaller than that of typical data sub-packet:

$$N_{row,\, with\, Ab}(d) \geq f_s T_{sub\_packet} = f_s/R_{DS} \qquad (17)$$

Consequently, the communication distance is limited as a function of the data sub-packet size with Ab as follows:

$$d \leq \frac{w \times R_{DS}}{f_s} \times (L/(2 \tan(\frac{FOV}{2}))) \qquad (18)$$

Within the maximum communication distance, the decoder shall also require the number of samples to clearly differentiate between the on and off state of the OOK or the VPPM signal in the time domain as expressed in (16).

Fig. 16(a) describes how data fusion is applied to collect and recover data from different images. Each data symbol shall be transmitted along with its clock information, allowing the camera decoder to group together images belonging to a data symbol. Each image provides a part of the data sub-packet; however, adjacent images are fused into a complete data subpacket. The fusion technique is beneficial in terms of distance because at a further distance the decoder operates well even if a part of the data recovered from the captured image is incomplete.

In Fig. 16(b), we present bit rate as a function of distance performances of the OOK modulation schemes. Our comparisons are performed against conventional OOK modulation formats, i.e. the data subpacket shall comprise a preamble and a payload. The fusion technique is implemented by inserting a single asynchronous bit at the start and end of each payload. OOK modulations using the fusion technique significantly outperform conventional OOK modulations. Specifically, at the same required data rate, the maximum distance is enhanced significantly with the fusion. Similarly, at the same required distance, the amount of actual information data is increased for each image (i.e. the subpacket payload after the overhead part is removed) and the fusion technique gains twice the data rate achieved by the typical technique.

IX. CONCLUSION AND DISCUSSION
In this study, we summarized the most recent works related to the OCC technology. Considering the high potential of OCC systems in enabling the next generation of wireless communication network, *i.e.*, 5G, we focused our discussion on the operation to link the technology to 5G. Specifically, we introduced novel OCC systems whose performance can be compared to those reported in other highlighted works. A detailed analysis of OCC system performance was compared to the findings of the related works in a comprehensive manner. Numerical analysis along with practical

simulations were newly introduced in this paper to provide the overview of OCC systems, their performance and suitable services. Also, the highly influential activity of the IEEE standardization TG7m was outlined. The inside look and evaluation of the technical proposals of OCC introduced in TG7m were also included in the performance analysis and comparison.

We classified OCC technologies into a set of five major types which address how the systems work and which LED Tx and camera Rx is applicable. The classification covered the entire research trend on OCC and current standardization of OCC TG7m. The image sensor model and the calculation of Eb/No based on the pixel amplitude value were addressed; this was helpful for the performance analysis and comparison.

The screen-based Nyquist sampling series operated at a low range of the optical clock rate (below 30Hz). We introduced two reference architectures for screen modulation and then analyzed our study and related research from different aspects (*i.e.*, the optical clock rate, MIMO, and channel coding). The high-framerate sampling series also follows Nyquist sampling. However, because of the requirement of flicker mitigation, high-speed cameras were used, which are best-applied in traffic light signals.

We have shared the great interest in the third category; Undersampled RoI signaling systems were designed being suitable for car-to-car communication, namely the killer app of OCC. The low-rate stream and high-rate data stream of RoI are simultaneously transmitted, making it a complete technology that is readily incorporated into cars. The performances of RoI signaling techniques were evaluated under dimming. The waveforms generation of RoI signals along with high-rate data stream were also described.

The hybrid OCC and PD systems were also described. The detection of light sources based solely on computer vision indicated a lower performance than the undersampled RoI signaling technique. In contrast, PD communication supported the required 5G data rate up to Gbps level using the advanced OFDM modulation series.

Finally, the rolling shutter sampling series were compared, and evaluated from different aspects. The tradeoff between data rate and distance which we newly analyzed in detail in this paper is fundamental but essential to any rolling shutter OCC system designer. The frequency modulation series and temporal modulation series were compared; the results suggested their suitable usages. The data fusion technique to extend the communication distance to twice the original value, and the frame rate variation support were also presented.

REFERENCES

[1] W. Xia, Y. Wen, C. H. Foh, D. Niyato, and H. Xie, "A survey on software-defined networking," *IEEE Commun. Surveys Tuts.*, vol. 17, no. 1, pp. 27–51, 1st Quart., 2015.

[2] B. A. A. Nunes, M. Mendonca, X.-N. Nguyen, K. Obraczka, and T. Turletti, "A survey of software-defined networking: Past, present, and future of programmable networks," *IEEE Commun. Surveys Tuts.*, vol. 16, no. 3, pp. 1617–1634, 3rd Quart., 2014.

[3] R. Horvath, D. Nedbal, and M. Stieninger, "A literature review on challenges and effects of software defined networking," *Procedia Comput. Sci.*, vol. 64, pp. 552–561, Oct. 2015.

[4] I. F. Akyildiz, P. Wang, and S.-C. Lin, "SoftAir: A software defined networking architecture for 5G wireless systems," *Comput. Netw.*, vol. 85, pp. 1–18, Jul. 2015.

[5] L. I. B. López, Á. L. V. Caraguay, L. J. G. Villalba, and D. López, "Trends on Virtualisation with software defined networking and network function Virtualisation," *IET Netw.*, vol. 4, no. 5, pp. 255–263, Sep. 2015.

[6] T. Wood, K. K. Ramakrishnan, J. Hwang, G. Liu, and W. Zhang, "Toward a software-based network: Integrating software defined networking and network function virtualization," *IEEE Netw.*, vol. 29, no. 3, pp. 36–41, May/Jun. 2015.

[7] P. H. Pathak, X. Feng, P. Hu, and P. Mohapatra, "Visible light communication, networking, and sensing: A survey, potential and challenges," *IEEE Commun. Surveys Tuts.*, vol. 17, no. 4, pp. 2047–2077, 4th Quart., 2015.

[8] N. Saha, M. S. Ifthekhar, N. T. Le, and Y. M. Jang, "Survey on optical camera communications: Challenges and opportunities," *IET Optoelectron.*, vol. 9, no. 5, pp. 172–183, Oct. 2015.

[9] L. Penubaku and K. Lakshmishree, "A survey on different techniques used for visible light communication," in *Proc. Int. Conf. Appl. Theor. Comput. Commun. Technol. (iCATccT)*, Davangere, India, Oct. 2015, pp. 783–786.

[10] N. T. Le, M. A. Hossain, A. Islam, D.-Y. Kim, Y.-J. Choi, and Y. M. Jang, "Survey of promising technologies for 5G networks," *Mobile Inf. Syst.*, vol. 2016, 2016, Art. no. 2676589.

[11] P. Pirinen, "A brief overview of 5G research activities," in *Proc. 1st Int. Conf. 5G for Ubiquitous Connectivity (5GU)*, Nov. 2014, pp. 17–22.

[12] N. Serafimovski *et al.*, *LiFi—Light Communications for 802.11*, document IEEE 802.11-16/1499r1, Nov. 2016.

[13] D. Tsonev, S. Videv, and H. Haas, "Towards a 100 Gb/s visible light wireless access network," *Opt. Exp.*, vol. 23, no. 2, pp. 1627–1637, Jan. 2015.

[14] (2017). *Official Website of IEEE 802.15.7m*, accessed on Mar. 28, 2017. [Online]. Available: http://www.ieee802.org/15/pub/IEEE%20802_15%20WPAN%2015_7%20Revision1%20Task%20Group.htm

[15] S. D. Perli, N. Ahmed, and D. Katabi, "PixNet: Interference-free wireless links using LCD-camera pairs," in *Proc. MobiCom ACM*, New York, NY, USA, 2010, pp. 137–148.

[16] T. Hao, R. Zhou, and G. Xing, "COBRA: Color barcode streaming for smartphone systems," in *Proc. MobiSys ACM*, New York, NY, USA, 2012, pp. 85–98.

[17] S. H. Chen and C. W. Chow, "Color-shift keying and code-division multiple-access transmission for RGB-LED visible light communications using mobile phone camera," *IEEE Photon. J.*, vol. 6, no. 6, pp. 1–6, Dec. 2014.

[18] N. Iizuka, *CASIO Response to 15.7r1 CFA*, document 15-15-0173r1, Mar. 2015, accessed on Mar. 28, 2017. [Online]. Available: https://mentor.ieee.org/802.15/dcn/15/15-15-0173-01-007a-casio-response-to-15-7r1-cfa.pdf

[19] S.-H. Chen and C.-W. Chow, "Hierarchical scheme for detecting the rotating MIMO transmission of the in-door RGB-LED visible light wireless communications using mobile-phone camera," *Opt. Commun.*, vol. 335, pp. 189–193, Jan. 2015.

[20] W. Hu, H. Gu, and Q. Pu, "LightSync: Unsynchronized visual communication over screen-camera links," in *Proc. 19th Annu. Int. Conf. Mobile Comput. Netw.*, New York, NY, USA, Oct. 2013, pp. 15–26.

[21] T. Nguyen and Y. M. Jang, "Novel 2D-sequential color code system employing image sensor communications for optical wireless communications," *ICT Exp.*, vol. 2, no. 2, pp. 57–62, Jun. 2016.

[22] (2016). *Revision on Kookmin Invisible Code*, accessed on Mar. 28, 2017. [Online]. Available: https://mentor.ieee.org/802.15/dcn/16/15-16-0802-01-007a-revision-on-kookmin-invisible-code.docx

[23] W. A. Cahyadi, Y. H. Kim, Y. H. Chung, and C.-J. Ahn, "Mobile phone camera-based indoor visible light communications with rotation compensation," *IEEE Photon. J.*, vol. 8, no. 2, Apr. 2016, Art. no. 7903308.

[24] G. Sharma, "Image-based data interfaces revisited: Barcodes and watermarks for the mobile and digital worlds," in *Proc. Int. Conf. Commun. Syst. Netw. (COMSNETS)*, Bangalore, India, Jan. 2016, pp. 1–6.

[25] Z. Yang, Z. Wang, J. Zhang, C. Huang, and Q. Zhang, "Wearables can afford: Light-weight indoor positioning with visible light," in *Proc. Int. Conf. Mobile Syst., Appl., Services*, 2015, pp. 317–330.

[26] Y. Long, S. Wang, W. Wu, X. Yang, G. Jeon, and K. Liu, "Structured-light-assisted wireless digital optical communications," *Opt. Commun.*, vol. 355, pp. 406–410, Nov. 2015.

[27] H. S. Liu and G. Pang, "Positioning beacon system using digital camera and LEDs," *IEEE Trans. Veh. Technol.*, vol. 52, no. 2, pp. 406–419, Mar. 2003.

[28] K. Ebihara, K. Kamakura, and T. Yamazato, "Spatially-modulated space-time coding in visible light communications using 2×2 LED array," in *Proc. IEEE Asia Pacific Conf. Circuits Syst. (APCCAS)*, Ishigaki, Japan, Nov. 2014, pp. 320–323.

[29] T. Nguyen, N. T. Le, and Y. M. Jang, "Asynchronous scheme for optical camera communication-based infrastructure-to-vehicle communication," *Int. J. Distrib. Sensor Netw.*, vol. 11, no. 5, May 2015.

[30] K. Ebihara, K. Kamakura, and T. Yamazato, "Layered transmission of space-time coded signals for image-sensor-based visible light communications," *J. Lightw. Technol.*, vol. 33, no. 20, pp. 4193–4206, Oct. 15, 2015.

[31] T. Nagura, T. Yamazato, M. Katayama, T. Yendo, T. Fujii, and H. Okada, "Improved decoding methods of visible light communication system for ITS using LED array and high-speed camera," in *Proc. IEEE Veh. Technol. Conf. (VTC)*, Taipei, Taiwan, May 2010, pp. 1–5.

[32] H. Okada, T. Ishizaki, T. Yamazato, T. Yendo, and T. Fujii, "Erasure coding for road-to-vehicle visible light communication systems," in *Proc. IEEE Consum. Commun. Netw. Conf. (CCNC)*, Las Vegas, NV, USA, Jan. 2011, pp. 75–79.

[33] R. D. Roberts, "A MIMO protocol for camera communications (Cam-Com) using undersampled frequency shift ON-OFF keying (UFSOOK)," in *Proc. IEEE Globecom Workshops (GC Wkshps)*, Atlanta, GA, USA, Dec. 2013, pp. 1052–1057.

[34] R. D. Roberts. *Intel Proposal in IEEE 802.15.7r1, Slide 1-129*, accessed on Mar. 28, 2017. [Online]. Available: https://mentor.ieee.org/802.15/dcn/16/15-16-0006-01-007a-intel-occ-proposal.pdf

[35] P. Luo, Z. Ghassemlooy, H. Le Minh, X. Tang, and H.-M. Tsai, "Under-sampled phase shift ON-OFF keying for camera communication," in *Proc. Int. Conf. Wireless Commun. Signal Process. (WCSP)*, Oct. 2014, pp. 1–6.

[36] P. Luo, Z. Ghassemlooy, H. Le Minh, H.-M. Tsai, and X. Tang, "Undersampled-PAM with subcarrier modulation for camera communications," in *Proc. Opto-Electron. Commun. Conf. (OECC)*, Shanghai, China, Jun. 2015, pp. 1–3.

[37] P. Luo *et al.*, "Experimental demonstration of RGB LED-based optical camera communications," *IEEE Photon. J.*, vol. 7, no. 5, Oct. 2015, Art. no. 7904212.

[38] T. Nguyen, A. Islam, and Y. M. Jang, "Region-of-interest signaling vehicular system using optical camera communications," *IEEE Photon. J.*, vol. 9, no. 1, Feb. 2017, Art. no. 7900720.

[39] (2016). *Kookmin University PHY sub-proposal for ISC using Dimmable Spatial M-PSK (DSM-PSK)*, accessed on Mar. 28, 2017. [Online]. Available: https://mentor.ieee.org/802.15/dcn/16/15-16-0015-02-007a-kookmin-university-phy-sub-proposal-for-isc-using-dimmable-spatial-m-psk-dsm-psk.pptx

[40] I. Takai, S. Ito, K. Yasutomi, K. Kagawa, M. Andoh, and S. Kawahito, "LED and CMOS image sensor based optical wireless communication system for automotive applications," *IEEE Photon. J.*, vol. 5, no. 5, Oct. 2013, Art. no. 6801418.

[41] I. Takai, T. Harada, M. Andoh, K. Yasutomi, K. Kagawa, and S. Kawahito, "Optical vehicle-to-vehicle communication system using LED transmitter and camera receiver," *IEEE Photon. J.*, vol. 6, no. 5, Oct. 2014, Art. no. 7902513.

[42] Y. Goto *et al.*, "BER characteristic of optical-OFDM using OCI," in *Proc. IEEE Asia Pacific Conf. Circuits Syst. (APCCAS)*, Ishigaki, Japan, Nov. 2014, pp. 328–331.

[43] Y. Goto *et al.*, "A new automotive VLC system using optical communication image sensor," *IEEE Photon. J.*, vol. 8, no. 3, Jun. 2016, Art. no. 6802716.

[44] C. Danakis, M. Afgani, G. Povey, I. Underwood, and H. Haas, "Using a CMOS camera sensor for visible light communication," in *Proc. IEEE Globecom Workshops*, Anaheim, CA, USA, Dec. 2012, pp. 1244–1248.

[45] Y. Liu *et al.*, "Light encryption scheme using light-emitting diode and camera image sensor," *IEEE Photon. J.*, vol. 8, no. 1, pp. 1–7, Feb. 2016.

[46] T. Nguyen, M. A. Hossain, and Y. M. Jang, "Design and implementation of a novel compatible encoding scheme in the time domain for image sensor communication," *Sensors*, vol. 16, no. 5, p. 736, May 2016.

[47] H. Aoyama and M. Oshima, "Visible light communication using a conventional image sensor," in *Proc. IEEE Consum. Commun. Netw. Conf. (CCNC)*, Las Vegas, NV, USA, Jan. 2015, pp. 103–108.

[48] H. Aoyama and M. Oshima, "Line scan sampling for visible light communication: Theory and practice," in *Proc. IEEE Int. Conf. Commun. (ICC)*, London, U.K., Jun. 2015, pp. 5060–5065.

[49] N. Rajagopal, P. Lazik, and A. Rowe, "Visual light landmarks for mobile devices," in *Proc. Int. Symp. Inf. Process. Sensor Netw. (IPSN)*, Berlin, Germany, 2014, pp. 249–260.

[50] H. Y. Lee, H. M. Lin, Y. L. Wei, H. I. Wu, H. M. Tsai, and K. C. J. Lin, "RollingLight: Enabling line-of-sight light-to-camera communications," in *Proc. Int. Conf. Mobile Syst., Appl., Services*, Florence, Italy, May 2015, pp. 167–180.

[51] *National Taiwan University 802-15-7r1 OCC Proposal*, accessed on Mar. 28, 2017. [Online]. Available: https://mentor.ieee.org/802.15/dcn/16/15-16-0018-00-007a-national-taiwan-university-802-15-7r1-occ-proposal.pdf

[52] C. H. Hong, T. Nguyen, N. T. Le, and Y. M. Jang, "Modulation and coding scheme (MCS) for indoor image sensor communication system," *Wireless Pers. Commun.*, pp. 1–17, Feb. 2017.

[53] Y. M. Jang, T. Nguyen, and H. C. Hyun. (2016). *Kookmin University PHY Sub-Proposal for ISC Using a Compatible M-FSK Scheme (CM-FSK)*, IEEE mentor 802.15. accessed on Mar. 28, 2017. [Online]. Available: https://mentor.ieee.org/802.15/dcn/16/15-16-0014-01-007a-kookmin-university-phy-sub-proposal-for-isc-using-a-compatible-m-fsk-scheme-cm-fsk.pptx

[54] *Kookmin University Comments to TCD 15-492r2: Flickering Consideration for OWC*, accessed on Mar. 28, 2017. [Online]. Available: https://mentor.ieee.org/802.15/dcn/15/15-15-0575-01-007a-kookmin-university-comments-to-tcd-15-492r2-flickering-consideration-for-owc.ppt

[55] *IEEE Standard for Local and Metropolitan Area Networks—Part 15.7: Short-Range Wireless Optical Communication Using Visible Light*, IEEE Standard 802.15.7 VLC 802.15.7-2011, accessed on Feb. 29, 2016. [Online]. Available: http://standards.ieee.org/findstds/standard/802.15.7-2011.html

[56] H. Haas, L. Yin, Y. Wang, and C. Chen, "What is LiFi?" *J. Lightw. Technol.*, vol. 34, no. 6, pp. 1533–1544, Mar. 15, 2016.

[57] C. Chen, D. A. Basnayaka, and H. Haas, "Downlink performance of optical attocell networks," *IEEE J. Lightw. Technol.*, vol. 34, no. 1, pp. 137–156, Jan. 1, 2016.

[58] M. S. Ifthekhar, N. T. Le, M. A. Hossain, T. Nguyen, and Y. M. Jang, "Neural network-based indoor positioning using virtual projective invariants," *Wireless Pers. Commun.*, vol. 86, no. 4, pp. 1813–1828, Feb. 2016.

[59] A. Ashok, S. Jain, M. Gruteser, N. Mandayam, W. Yuan, and K. Dana, "Capacity of screen–camera communications under perspective distortions," *Pervasive Mobile Comput.*, vol. 16, pp. 239–250, Jan. 2015.

[60] (2015). *Offline to Online Marketing*, accessed on Mar. 28, 2017. [Online]. Available: https://mentor.ieee.org/802.15/dcn/15/15-15-0445-00-007a-offline-to-online-marketing.pdf

[61] A. Islam, M. A. Hossain, T. Nguyen, and Y. M. Jang, "High temporal-spatial resolution optical wireless communication technique using image sensor," in *Proc. Int. Conf. Inf. Commun. Technol. Converg. (ICTC)*, Jeju, Oct. 2016, pp. 1165–1169.

[62] T. Li, C. An, X. Xiao, A. T. Campbell, and X. Zhou, "Real-time screen-camera communication behind any scene," *MobiSys*, May 2015, pp. 197–211.

TRANG NGUYEN received the B.E. degree major in biomedical electronics engineering from the School of Electronics and Telecommunications, Hanoi University of Science and Technology, Vietnam, in 2013, and the M.S. degree from Kookmin University (KMU) in 2015, where he is currently pursuing the Ph.D. degree. He is also a Researcher with the LED Convergence Research Center, KMU. His interested research areas include biomedical electronics, optical camera communications, localization, digital signage, and augmented reality services. He is also a Voting Member of the IEEE 802.15.7m Task Group.

AMIRUL ISLAM received the B.Sc. degree in electrical and electronic engineering from the Khulna University of Engineering and Technology, Bangladesh, in 2014. He is currently pursuing the M.Sc. degree in electronics engineering with Kookmin University, South Korea. His research interests include optical camera communication, location-based services, automotive optical vehicular communication, 5G networking, and artificial intelligence.

MD. TANVIR HOSSAN was born in Barisal, Bangladesh, in 1991. He received the B.Sc. degree in electrical and electronic engineering from the Khulna University of Engineering & Technology, Bangladesh, in 2013. He is currently pursuing the master degree in electronics engineering with Kookmin University, South Korea. His research interests include optical wireless communication, optical camera communication, location based services, digital signage, and artificial intelligence.

YEONG MIN JANG received the B.E. and M.E. degrees in electronics engineering from Kyungpook National University, South Korea, in 1985 and 1987, respectively, and the Doctoral degree in computer science from the University of Massachusetts, USA, in 1999. He was with the Electronics and Telecommunications Research Institute (ETRI) from 1987 to 2000. Since 2002, he has been with the School of Electrical Engineering, Kookmin University, Seoul, South Korea, where he has been the Director of the Ubiquitous IT Convergence Center, since 2005, and the Director of the LED Convergence Research Center, since 2010. He is currently a Life Member of the Korean Institute of Communications and Information Sciences (KICS). He received the Young Science Award from the Korean Government (2003–2006). He has organized several conferences and workshops, such as the International Conference on Ubiquitous and Future Networks (2009–2016), the International Conference on ICT Convergence (2010–2016), the International Conference on Information Networking 2015, and the International Workshop on Optical Wireless LED Communication Networks (2013–2016). He had served as the Founding Chair of the KICS Technical Committee on Communication Networks in 2007 and 2008. He had served as the Executive Director of KICS from 2006 to 2014 and Vice President of KICS from 2014 to 2016. He serves as the Co-Editor-in-Chief of *ICT Express,* which is published by Elsevier. He had been the Steering Chair of the Multi-Screen Service Forum since 2011, and the Society Safety System Forum since 2015. He had served as the Chairman of the IEEE 802.15 Optical Camera Communications Study Group in 2014. He is currently serving as the Chairman of the IEEE 802.15.7m Optical Wireless Communications Task Group. He is also the Chairman of IEEE 802.15 Vehicular Assistive Technology (VAT) Interest Group. His research interests include 5G mobile communications, multi-screen convergence, public safety, optical wireless communications, optical camera communication, and Internet of Things.

• • •